Modelling load transfer in single-lap adhesively bonded and hybrid (bolted / bonded) joints

Eric Paroissien, Frederic Lachaud, Sébastien Schwartz

Modelling load transfer in single-lap adhesively bonded and hybrid (bolted / bonded) joints

Eric Paroissien [a,*], Frédéric Lachaud [a], Sébastien Schwartz [a,b]

[a] Institut Clément Ader (ICA), Université de Toulouse, ISAE-SUPAERO, INSA, IMT MINES ALBI, UTIII, CNRS, 3 Rue Caroline Aigle, 31400, Toulouse, France
[b] ISAE-SUPAERO, 10 Avenue Edouard Belin, Toulouse, 31400, France

Keywords:
Load transfer
Adhesively bonded joint
Hybrid (bolted
Bonded) joints
Single-lap joint
Closed-form solutions
Semi-analytical resolution
Macro-element modelling
Cohesive zone modelling

A B S T R A C T

An aerospace structure is built from the assembly of structural sub-components involving joining technologies such as welding, mechanical fastening or adhesive bonding.

The function of joints is to ensure load transfer between the structural sub-components. The integrity of the structure directly depends on strength of these joints. In order to design these critical structural areas, load transfer between structural sub-components must be assessed. The objective of this review paper is to present approaches for the simplified modelling and associated resolution schemes of single-lap adhesively bonded and hybrid (bolted/bonded) joints to predict load transfer. We show that the scope of available closed-form solutions is restricted, such that the use of semi-analytical schemes is suitable. Macro-element modelling is then presented. This technique allows the assessment of load transfer and associated stresses, especially in the adhesive layer regarded as a cohesive zone, while enabling the enrichment of the model, making it more representative of the physical reality.

1. Introduction

Assemblies remain compulsory in the design of aerospace structures. Numerous joining technologies are used in aerospace construction such as welding, mechanical fastening or adhesively bonded joints [1,2] for example. The main function of joints is to enable the physical existence of the structure, consisting of structural sub-components. In-service, the structure is subjected to external loads that it must be able to withstand while performing the expected functions. These external loads are then distributed through the structural sub-components in the shape of internal loads whose nature depends on the initial particular design choices. The structural sub-components are then sized to withstand these internal loads. The mechanical function of joints is then to ensure the balance of structural sub-components subjected to internal loads. Indeed, the fastening elements, such as an adhesive layer or a rivet, are thus subjected to the reaction of internal loads. These fastening elements experience deformation, resulting in a stress field to balance the applied internal loads. As a result, the deformation of fastening elements serves to balance structural sub-components, a phenomenon known as load transfer. This paper focuses on adhesive bonding – simply termed bonding. Only the commonly used design solution of the single-lap joint is addressed in this paper. Moreover, as aerospace structures are mainly built from thin shells reinforced by beams, the single-lap joint is assumed to be made of two slender and flat structural sub-components – simply termed adherends.

The load transfer within a single-lap bonded joint is illustrated in Fig. 1(a–c). The adherends are subjected to a pair of tensile loads applied at both extremities. To simplify, the kinematics are restricted to longitudinal displacements in the adherends. The relative difference between the longitudinal displacements of both adherend interfaces induces a shear deformation of the adhesive layer along the entire adhesive layer. This means that load transfer is performed by the shearing of the adhesive layer, such as explicitly represented by de Bruyne in the figures labelled “cinema picture” [2]. If the adherends were infinitely rigid, the shear deformation in the adhesive layer would be constant along the overlap. But the adherends are deformable and induce a gradient of shear deformation in the adhesive layer along the overlap (Fig. 2 (a)). This load transfer mode is continuous because it is performed along the entire overlap [3]. This was mathematically described by Arnovljevic in 1909 [4] and by Volkersen in 1938 [5] by considering the differential tension in the adherends due to the shear strain in the adhesive layer, termed shear-lag. It is interesting to note that, in their paper, Arnovljevic and Volkersen [4,5] developed an analogy to assess the bolt load transfer

* Corresponding author.
E-mail address: eric.paroissien@isae-supaero.fr (E. Paroissien).

https://doi.org/10.1016/j.paerosci.2022.100811

Nomenclature and units

A_i	extensional stiffness (N) of adherend i
$\mathscr{A}$	matrix of the governing system of ODEs
B_i	extensional and bending coupling stiffness (N.mm) of adherend i
C	vector of integration constants
C_F	fastener stiffness (N.mm^{-1})
C_j	stiffness (N.mm^{-1}) of the jth fastener
C_u	fastener stiffness (N.mm^{-1}) component in the x direction
C_{u1}	first fastener stiffness (N.mm^{-1}) component in the x direction
C_{u2}	second fastener stiffness (N.mm^{-1}) component in the x direction
C_v	fastener stiffness (N.mm^{-1}) component in the y direction
$C\theta$	fastener stiffness (N.mm) component around the z direction
$\overline{\boldsymbol{C}}$	stiffness (N.mm)
D_e^{-1}, $D'_e{}^{-1}$	coupling matrices
D_i	bending stiffness (N.mm^2) of adherend i
E	adhesive peel modulus (MPa)
$E_{a,min}$	adhesive shear modulus (MPa)
$E_{a,max}$	adhesive shear modulus (MPa)
E_i	Young's modulus (MPa) of adherend i
E_f	screw Young's modulus (MPa)
E_r	adherend Young's modulus (MPa)
F_e	elementary nodal force vector
F_s	structural nodal force vector
$F_{e,therm}$	elementary nodal force vector equivalent to thermal load
G	adhesive shear modulus (MPa)
G_i	adherend shear modulus (MPa) of adherend i
K_e	elementary stiffness matrix
K_e	elementary stiffness of fastener ME
K_s	structural stiffness matrix
L_e, L'_e	coupling matrices
$K_{bar,i}$	elementary stiffness matrix of a bar element for the adherend i
$K_{beam,i}$	elementary stiffness matrix of a beam element for the adherend i
K_j	integration constants (j = 1..13)
L	length (mm) of bonded overlap
M_i	bending moment (N.mm) in adherend i around the z direction
$M_i^{\Delta_T}$	thermal bending moment (N.mm) in adherend i around the z direction
N	truncation order
N_i	normal force (N) in adherend i in the x direction
$N_{i,j}$	normal force (N) in adherend i and bonded sandwich j in the x direction
$N_i^{\Delta_T}$	thermal normal force (N) in adherend i in the x direction
$Q_i^{P_i}$	reduced modulus (MPa) along the x direction of the p_i^{th} ply of adherend i
R_i	parameters (i = 1,2,3)
S	adhesive peel stress (MPa)
T	adhesive shear stress (MPa)
T_{av}	average adhesive shear stress (MPa)
$T_{\max}$	maximum adhesive shear stress (MPa)
T_c	critical adhesive shear stress (MPa)
U_e	elementary nodal displacement vector
U_s	structural nodal displacement vector
V_i	shear force (N) in adherend i in the y direction
b	adherend half-width (mm)
c	overlap half-length (mm)
c_k	integration constant
d_j	abscissa (mm) of the jth fastener
e	thickness (mm) of the adhesive layer
e_i	thickness (mm) of the adherend i
e_r	thickness (mm) of the adherend
f	magnitude of applied tensile force (N)
f_c	magnitude of critical applied tensile force (N)
h_i	half thickness (mm) of adherend i
h_r	half thickness (mm) of the adherend
h	difference (mm) between h_1 and h_2
h_+	sum (mm) of h_1 and h_2
k'	parameter
k_{GR}	bending moment factor according to Goland and Reissner
k_M	bending moment factor
k_{lap}	stiffness (N.mm^{-1}) in the x direction of the overlap
k_{joint}	stiffness (N.mm^{-1}) in the x direction of the joint
k_j	constant (j = 1..4)
l_i	length outside of the overlap (mm) of the adherend i
n	number of fasteners
$\overline{q}$	parameter
r, r'	real number in mm^{-1}
$\overline{r}$	parameter
s, s'	real number in mm^{-1}
t, t'	real number in mm^{-1}
u_f	total displacement (mm) of the joint in the x direction
u_i	displacement (mm) of adherend i in the x direction
$u_{[i]}$	nodal displacement (mm) of node i
v_i	displacement (mm) of adherend i in the y direction
w	adherend width (mm)
Δ	overlap length (mm) of a macro-element
Δ_T	temperature variation (K)
Δ_j	characteristic parameter (N^2.mm^2) of adherend i
$\varphi_{\mathscr{A}}$	fundamental matrix of $\mathscr{A}$
α_i	coefficient of thermal expansion (K^{-1}) of adherend i
$\alpha_i^{P_i}$	coefficient of thermal expansion (K^{-1}) of the p_i^{th} ply adherend i
β	characteristic argument
δ_{u1}	axial displacement (mm) limiting the first phase of a fastener bilinear law
φ	applied tensile flow (N.mm^{-1})
φ_j	parameter associated with the jth fastener
φ_c	critical tensile flow (N.mm^{-1})
η	characteristic argument (mm^{-1})
κ	parameter (mm.MPa^{-1}) involved in the shear correction factor
λ	characteristic argument
ν	adhesive Poisson's ratio
ν_f	screw Poisson's ratio
ν_r	adherend Poisson's ratio
θ_i	bending angle (rad) of the adherend i around the z direction
τ_j	bolt load transfer rate of the jth fastener
ξ	adherend stiffness unbalance parameter (−)
$\xi\alpha$	adherend thermal expansion unbalance parameter (−)
χ	adherend stiffness unbalance parameter (−)
ω	characteristic argument (mm^{-1})
(x,y,z)	global reference system of axes
CZM	cohesive zone model
DoF	degree of freedom
FE	Finite Element
HBB	hybrid (bolted/bonded)
ME	macro-element
ODE	ordinary differential equation
TEPS	Taylor expansion in power series
1D	one-dimensional
2D	two-dimensional
3D	three-dimensional

rate within a bolted joint. For the purposes of comparison, the shear deformation of fasteners allows for load transfer within a single-lap bolted joint (Fig. 1(d–f)). Contrary to bonded joints, this load transfer mode is discrete as it occurs at the fastener location [3]. In the context of research projects led by NACA and published in 1946 and 1947 [6–8], it was shown that load transfer is not uniformly distributed on the fasteners similarly to bonded joints (Figs. 1 and 2).

Modelling consists in idealizing the physical reality by choosing simplifying hypotheses. These simplifying hypotheses are then translated into a set of mathematical equations and must be solved. A purely analytical resolution, leading to a closed-form meaning ready-to-use equation, could be possible if the simplifying hypotheses are sufficiently strong. If these hypotheses are too strong however, in other words out of phase with the physical reality, the results could be significantly different from the experimental results observed. When formal treatment by hand of equations is not possible, this is due to the hypotheses that are less strong. A semi-analytical approach can then be employed, consisting in a resolution scheme based on more or less elementary numerical schemes. The results are obtained through a dedicated computer program. Finally, when a choice reasonably relevant to the physical reality can no longer be made, advanced numerical methods such as the Finite Element (FE) method can be used. If suitably applied, these numerical methods can give results close to experimental measurements, after processing times longer than analytical and semi-analytical methods. Even though computer performance is continuously being improved, the *simplified analyses*, which gather the models associated with analytical or semi-analytical resolution schemes, remain attractive. Indeed, they offer the ability to make quick decisions at low cost and can be embedded in the framework of iterative computation processes such as those used to take into account nonlinearities and to feed optimization and/or probabilistic computation loops.

Based on existing theories available in the literature – often developed for aerospace applications, but also for applications in the field of the civil construction or electronic devices – the objective of this paper is to provide a comprehensive review of modelling approaches for the simplified analysis of single-lap bonded joints in connection with the associated resolution schemes. The simplified analysis of bonded joints can be sorted into two families. In the first family, the adherends are seen as bars, beams or plates in cylindrical bending linked by an elastic foundation modelling the adhesive layer; this family thus consists of one-dimensional models. The model by Arnovljevic [4] or Volkersen [5] belongs to this family.

Considering the adhesive layer as an elastic foundation allows the deformation and the stress of the adhesive to be expressed as a function of the displacement and rotation of adherends. In other words the adhesive layer is seen as a coupling of the kinematics of adherends, so that the local equilibrium of the adhesive is not taken into account. The models belonging to the second family consider the sandwich as a plane continuum elastic medium, such that the local equilibrium of the adhesive layer is included. The effort in the mathematical processing

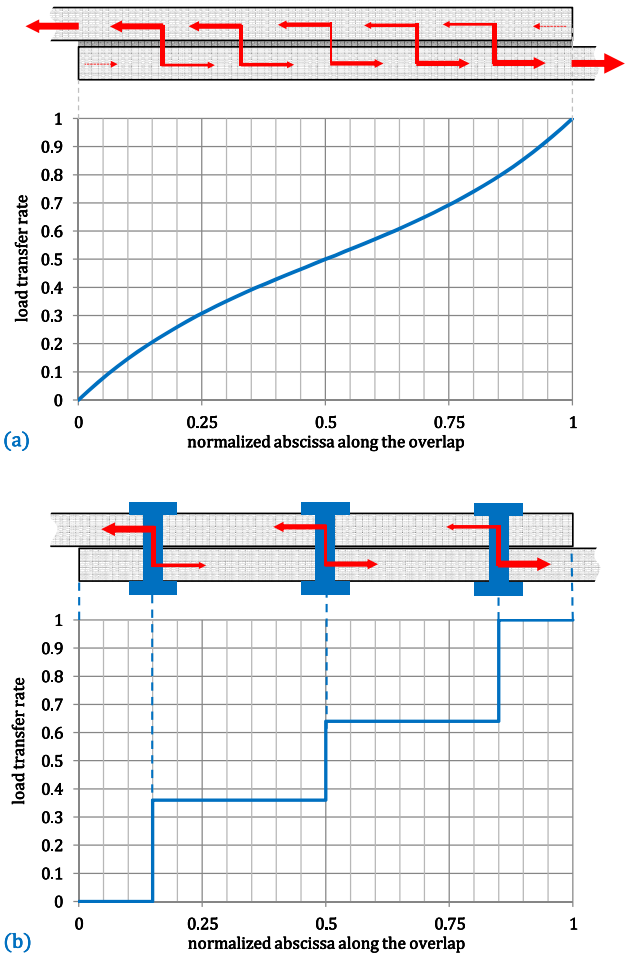

Fig. 2. Load transfer in a single-lap bonded (a) joint (a) and in a single-lap bolted joint (b).

associated with the one-dimensional (1D) models of the first family appears to be less significant than the one required of the potentially two-dimensional (2D) models of the second family. However, this paper will show that the ability to write a closed-form solution for the models using an elastic foundation for the adhesive is not always possible, in particular when the kinematics of adherends include in-plane and out-of-plane components. Finally, a particular semi-analytical method, called macro-element (ME) modelling, is emphasized and applied to a more complex configuration: the single-lap hybrid (bolted/bonded), quoted HBB, joint, combining an adhesive layer and fasteners.

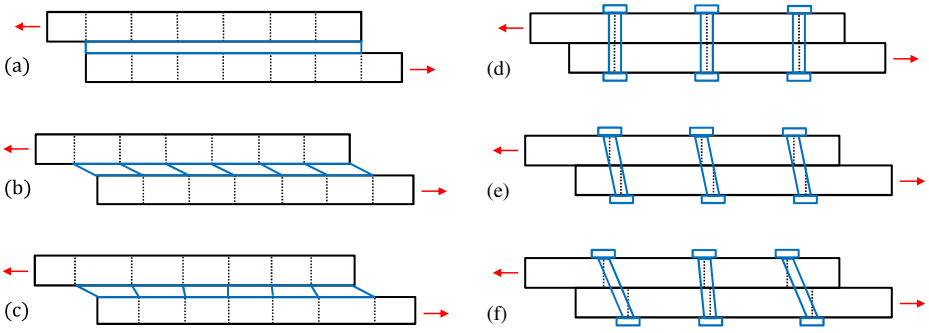

Fig. 1. Load transfer in a single-lap bonded (bolted) joint (a(d)) initial configuration, (b(e)) final configuration with infinitely rigid adherends, (c(f)) final configuration with deformable adherends.

2. Fundamental models

2.1. Shear-lag approach

2.1.1. Simplifying hypotheses and governing equations

The model presented by Arnovljevic or Volkersen [4,5] for the analysis of a single-lap bonded joint subjected to tensile load quoted *f* at one extremity and clamped at the other one (Fig. 3) is a shear-lag model. The simplifying hypotheses are:

i. Under quasi-static loading;
ii. Homogeneous linear elastic isotropic materials;
iii. The adherends are seen as bars;
iv. The adhesive layer is seen as a homogeneous elastic foundation at one parameter associated with shearing and linking both adherend interfaces;
v. The geometrical parameters are constant.

The geometric and material parameters are free and assumed strictly positive to have a physical meaning. This set of simplifying hypotheses implies that all the components of the adherend (adhesive) stress tensor can be neglected compared to the normal (shear) component. The model framework is then called *1D-bar*. Moreover, the adhesive shear component is constant through the layer thickness. From these hypotheses, the constitutive equations and the local equilibrium equations of adherends (Fig. 3) lead to the governing system of first-order ordinary differential equations (ODEs) written as follows:

$$\begin{cases} \dfrac{dN_i}{dx} = (-1)^i 2bT \\ \dfrac{du_i}{dx} = \dfrac{N_i}{A_i} \end{cases} \qquad i = 1,2 \tag{1}$$

where N_i and u_i are the unknown functions denoting, for the adherend i, for the normal force and the longitudinal displacement of a point located before deformation at the abscissa x on the neutral line. A_i is the membrane stiffness of the adherend i and $w=2b$ is the width of each adherend. The adhesive shear stress T couples the constitutive and local equilibrium equations. This takes the following shape:

$$T = \frac{G}{e}(u_2 - u_1) \tag{2}$$

where G is the adhesive shear modulus and e is the adhesive layer thickness.

2.1.2. Resolution

The governing system of equations in Eq. (1) can be analytically solved. The expressions for the adherend longitudinal displacements involve four integration constants c_1, c_2, c_3 and c_4:

$$\begin{pmatrix} u_1(x) \\ u_2(x) \end{pmatrix} = \frac{1}{2}\begin{pmatrix} 1 & x & -(1+\chi)e^{-\eta x} & -(1+\chi)e^{\eta x} \\ 1 & x & (1-\chi)e^{-\eta x} & (1-\chi)e^{\eta x} \end{pmatrix}\begin{pmatrix} c_1 \\ c_2 \\ c_3 \\ c_4 \end{pmatrix} \tag{3}$$

where:

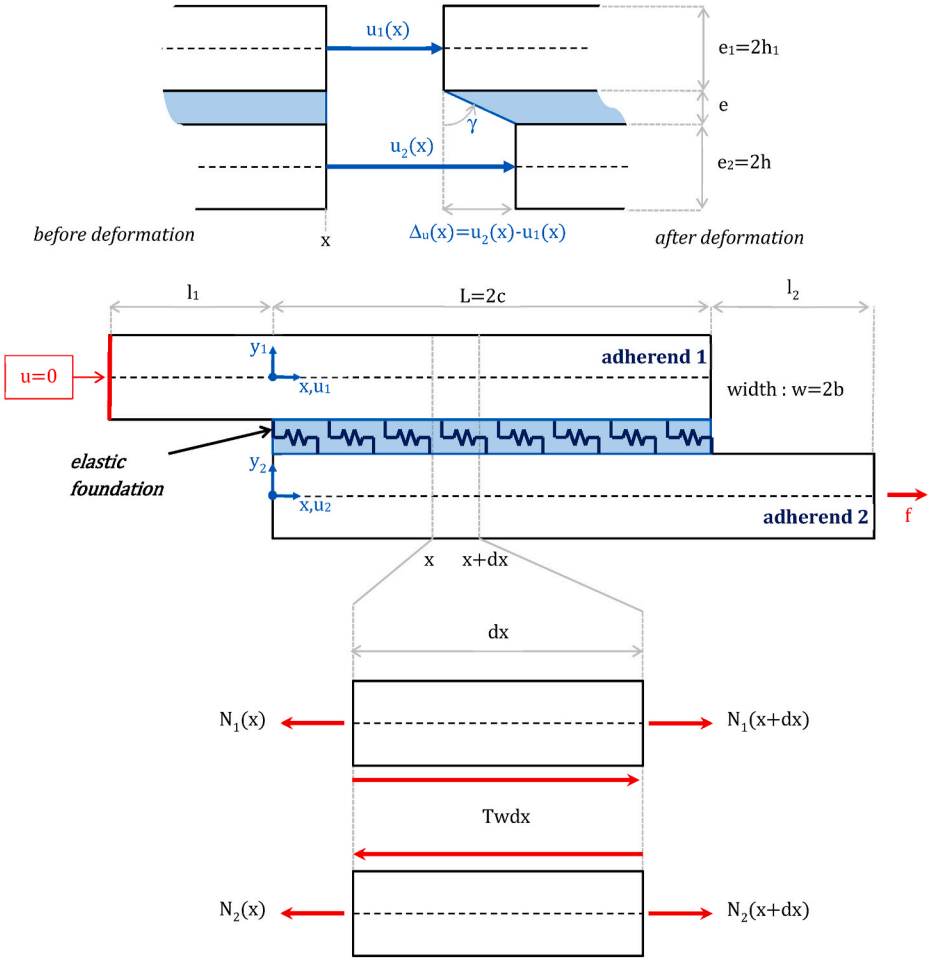

Fig. 3. Kinematics, parameterization and local equilibrium of the single-lap bonded joint under 1D-bar modelling.

$$\eta^2 = \frac{G}{e}\frac{1+\xi}{e_2E_2} = \frac{G}{e}\left(\frac{1}{e_1E_1}+\frac{1}{e_2E_2}\right) \tag{4}$$

$$\chi = \frac{\frac{1}{e_1E_1}-\frac{1}{e_2E_2}}{\frac{1}{e_1E_1}+\frac{1}{e_2E_2}} = \frac{\xi-1}{\xi+1} \tag{5}$$

$$\xi = \frac{e_2E_2}{e_1E_1} \tag{6}$$

and e_i and E_i are respectively the thickness and the Young's modulus of the adherend i. Due to the constitutive equations of the adherend, the expression for the adherend normal forces depends solely on c_2, c_3 and c_4:

$$\begin{pmatrix} N_1(x) \\ N_2(x) \end{pmatrix} = \frac{1}{2}\begin{pmatrix} 0 & A_1 & \eta(1+\chi)A_1e^{-\eta x} & -\eta(1+\chi)A_1e^{\eta x} \\ 0 & A_2 & -\eta(1-\chi)A_2e^{-\eta x} & \eta(1-\chi)A_2e^{\eta x} \end{pmatrix}\begin{pmatrix} c_1 \\ c_2 \\ c_3 \\ c_4 \end{pmatrix} \tag{7}$$

The length of the overlap is denoted $2c$. Considering that the normal force of adherend 2 is equal to 0 in $x=0$ and is equal to f in $x=2c$, as well as that the global equilibrium relationship $N_1+N_2=f$ for every x, the expressions for c_2, c_3 and c_4 are:

$$\begin{cases} c_2 = (1+\chi)\dfrac{f}{A_2} \\ c_3 = \dfrac{1}{\eta}\dfrac{1+\xi e^{2\omega}}{4\sinh 2\omega}\dfrac{f}{A_2} \\ c_4 = \dfrac{1}{\eta}\dfrac{1+\xi e^{-2\omega}}{4\sinh 2\omega}\dfrac{f}{A_2} \end{cases} \tag{8}$$

where:

$$\omega = \eta c = \frac{\sqrt{\frac{G2bc}{e}}}{\sqrt{\frac{1}{1+\xi}\frac{E_2 2be_2}{c}}} \tag{9}$$

The expression for the adhesive shear stress as a function of the average shear stress along the overlap $<T>_{2c} = T_{av} = f/(2b.2c)$ requires c_3 and c_4 only to be established and is such as:

$$T = \frac{\omega}{1+\xi}\left(\frac{1+\xi e^{2\omega}}{2\sinh 2\omega}e^{-\eta x}+\frac{1+\xi e^{-2\omega}}{2\sinh 2\omega}e^{\eta x}\right)T_{av} \tag{10}$$

As expected, the displacement field given in Eq. (3) is known within the constant c_1. In the case of the single-lap bonded joint, the longitudinal displacement of adherend 1 in $x=0$ is equal to $(f/A_1)l_1$, so that:

$$u_1(0) = \frac{f}{A_1}l_1 = \frac{1}{2}[c_1-(1+\chi)(c_3+c_4)] \Rightarrow c_1 = \left[\frac{2\xi l_1}{c}+\frac{\xi}{1+\xi}\left(\frac{1+\xi\cosh 2\omega}{2\omega\sinh 2\omega}\right)\right]\frac{f}{A_2}c \tag{11}$$

where l_1 is the length of the adherend 1 outside the overlap.

2.1.3. Particular results

Stiffness. Owens and Lee-Sullivan [9] provided a semi-analytical approach for the determination of the stiffness of single-lap bonded joints. This model is inspired by the model for the assessment of bolt load transfer rate developed at NACA in the 1940s [6–8]. Indeed, the bonded overlap is regarded as the series of elementary cells, each composed by one spring representing each of both adherends and two springs for the adhesive layer. The relative displacement of each elementary cell is computed using the Adams and Peppiatt [10,11] simplified 1D-bar analysis of bonded joints, which includes adherend shearing. In 2004, Xiao et al. [12] provided an analytical formula for the stiffness of a double-lap joint, allowing out-of-plane displacement to be neglected and assuming a constant shear strain along the bonded overlap. The deformability of adherends then appears negligible (Fig. 1(b)). In 2018, Li et al. [13] derived an analytical formula for the stiffness of quadruple bonded overlap taken into account for the elasticity of both the adhesive layer and adherends following the model of Arnovljevic or Volkersen. In a manner similar to Li et al. and from the given in the previous section attached to the shear-lag model of Arnovljevic or Volkersen, the stiffness of a single-lap bonded joint can be determined. The relative displacement of the overlap is then written as:

$$u_2(2c)-u_1(0) = \left[1+\frac{1}{2}\left(\frac{2+\left(\frac{1+\xi^2}{\xi}\right)\cosh 2\omega}{2\omega\sinh 2\omega}\right)\right]\left(\frac{\xi}{1+\xi}\frac{f}{A_2}\right)2c \tag{12}$$

The stiffness of the overlap k_{lap} under a tensile load f is then:

$$k_{lap} = \left[1+\frac{1}{2}\left(\frac{2+\left(\frac{1+\xi^2}{\xi}\right)\cosh 2\omega}{2\omega\sinh 2\omega}\right)\right]^{-1}\left(\frac{1+\xi}{\xi}\right)\left(\frac{A_2}{2c}\right) \tag{13}$$

The longitudinal displacement of the application point of f is termed u_f. It represents the total displacement of the joint in the x-direction. As u_f-$u_2(2c) = (f/A_2)l_2$, where l_2 is the length of the adherend 2 outside the overlap, the expression for u_f is given by:

$$u_f = \left[\xi l_1+\frac{\xi}{1+\xi}\left(1+\frac{1}{2}\left(\frac{2+\left(\frac{1+\xi^2}{\xi}\right)\cosh 2\omega}{2\omega\sinh 2\omega}\right)\right)2c+l_2\right]\left(\frac{f}{A_2}\right) \tag{14}$$

The stiffness of the joint, quoted k_{joint}, is then given by:

$$k_{joint} = \left[\frac{\xi l_1+l_2}{2c}+\frac{\xi}{1+\xi}\left(1+\frac{1}{2}\left(\frac{2+\left(\frac{1+\xi^2}{\xi}\right)\cosh 2\omega}{2\omega\sinh 2\omega}\right)\right)\right]^{-1}\left(\frac{A_2}{2c}\right) \tag{15}$$

These formulae allow the creation of a simple model of the single-lap joint with simple springs. There is only one spring if k_{joint} is used or 3 springs if k_{lap} is used, as illustrated in Fig. 4.

Load transfer and adhesive stress. The shear-lag model solution shows that the load transfer is not uniformly distributed along the overlap (Fig. 2(a)). Adhesive peak shear stresses are located at both overlap extremities with values given by:

$$\begin{cases} T(0) = \dfrac{\omega}{1+\xi}\left(\dfrac{1+\xi\cosh 2\omega}{\sinh 2\omega}\right)T_{av} \\ T(2c) = \dfrac{\omega}{1+\xi}\left(\dfrac{\cosh 2\omega+\xi}{\sinh 2\omega}\right)T_{av} \end{cases} \tag{16}$$

This means that the load transfer is more intense at both overlap extremities. It is useful to note that the area under the shear stress distribution along the overlap is equal to the tensile flow $\varphi = f/2b$ to be transferred by the bonded joint; this result comes from the integration along the overlap length of the local equilibrium equation of adherends in Eq. 1.

In the case where the joint is balanced, meaning that both adherends have a membrane stiffness ($\xi = 1$), the adhesive shear stress distribution is symmetrical with respect the centre of the overlap (see Fig. 5). The values of the stress peaks are the same, such that the ratio between the maximal stress $T_{\max}$ with the average shear stress reads:

$$\frac{T_{max}}{T_{av}} = \frac{\omega}{\tanh\omega} \tag{17}$$

The parameter ω drives the adhesive shear stress distribution along the overlap. It is formed by the ratio between a term relative to the adhesive layer shear stiffness with a term relative to the membrane stiffness of both adherends. For a prescribed average applied shear stress T_{av}, the maximal adhesive shear stress $T_{\max}$ is a strictly increasing function of ω. When ω tends towards 0 (e.g. flexible adhesive layer) $T_{\max}$ tends towards T_{av}, meaning that the shear stress distribution tends to be

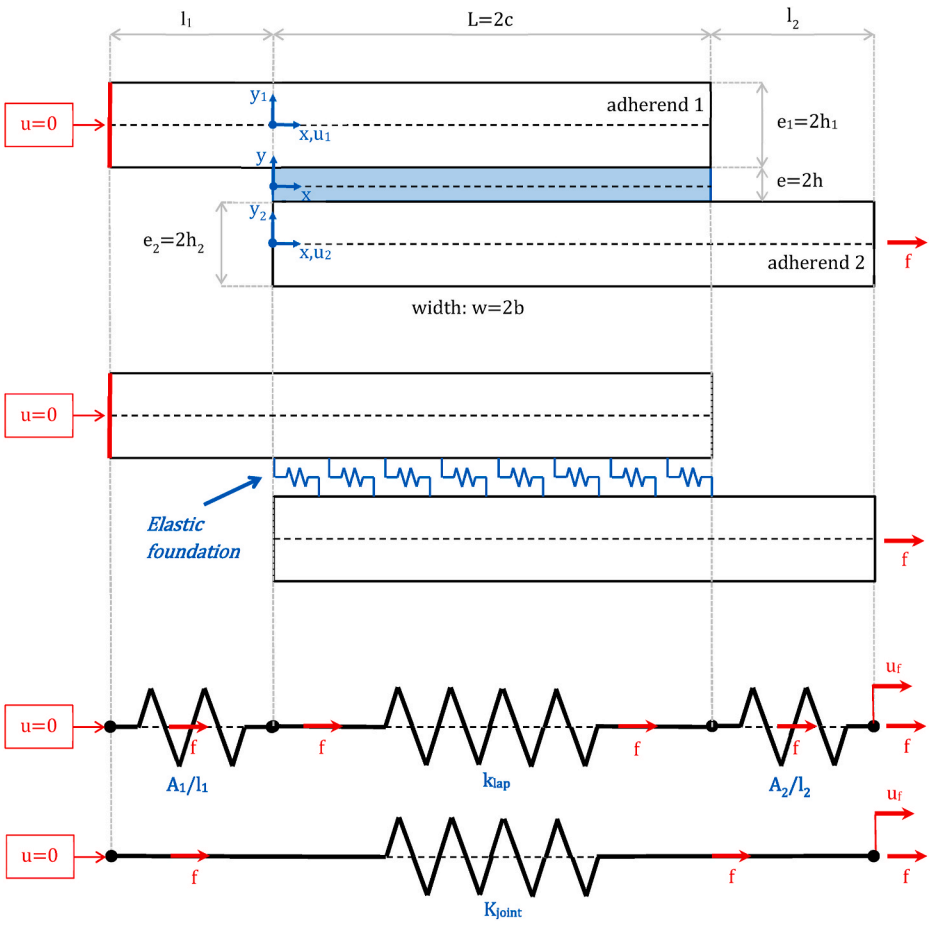

Fig. 4. Spring models of a single-lap bonded joint.

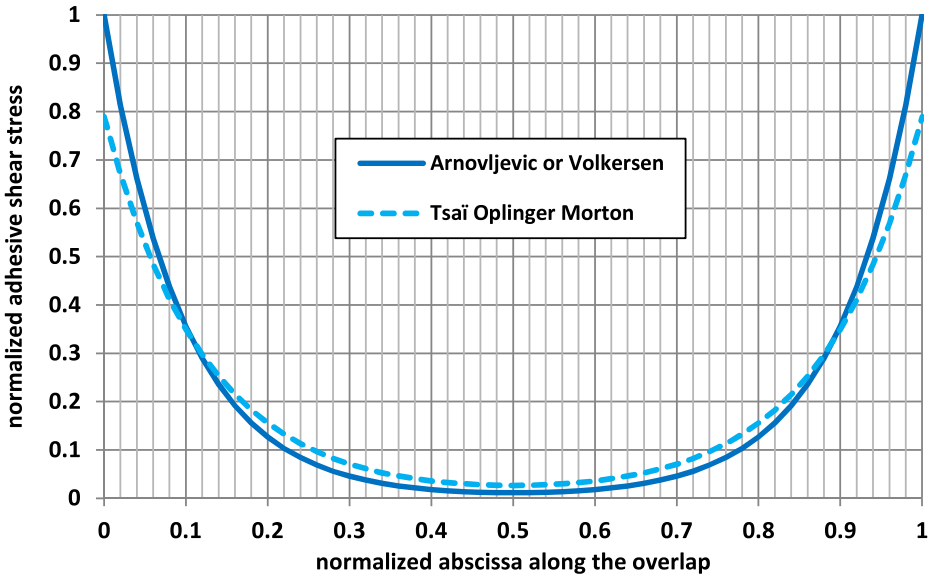

Fig. 5. Normalized shear stress as a function of normalized abscissa in the case of a balanced joint. The maximum shear stress from the Arnovljevic or Volkersen model (Eq. (17)) is taken to normalize the shear stress distribution. Parameters used: $e_1 = e_2 = 2$ mm, $2c = w = 25$ mm, $E_1 = E_2 = 70$ GPa, $\nu_1 = \nu_2 = 0.33$, $G/e = 11950$ MPa mm^{-1}, $f = 5$ kN.

uniform along the overlap leading to a linear distribution of the load transfer from 0 to f. The *Thick Adherend Shear Test* (ISO 11003-2:2019) [14], aims to provide an experimental measurement of the adhesive shear stress strain curve and of an adhesive critical shear stress T_c, which benefits from this behaviour at small ω. When ω tends towards infinity (e.g. rigid adhesive layer) T_{max} tends towards infinity. If it is assumed that a failure criterion for the adhesive layer consist in ensuring that T_{max} is lower than T_c, it is not possible to indefinitely stiffen the joint

without leading to the failure of this latter. Moreover, from the equation Eq. (17), Volkersen [15] showed that the critical tensile flow to be transferred at failure quoted $\varphi_c = f_c/2b$, is given by:

$$\varphi_c = \frac{f_c}{2b} = 2\frac{\tanh\omega}{\eta}T_c \tag{18}$$

$$T = \frac{\omega}{\sinh\omega}T_{av}\cosh\left(\omega\left[\frac{x}{c}-1\right]\right) + \frac{\eta}{2b}\frac{1}{\cosh\omega}\left[\left(\frac{1}{2}-\frac{\xi}{1+\xi}\right)f + \frac{\left(1-\frac{1}{\xi_\alpha}\right)}{1+\xi}A_2\alpha_2\Delta_T\right]\sinh\left(\omega\left[\frac{x}{c}-1\right]\right) \tag{19}$$

where f_c is the critical load. The critical tensile flow appears to increase strictly with the overlap length $2c$ and is bounded by $2T_c/\eta$. In other words, the increase in overlap length increases the load level, which can be transmitted up to a fixed asymptotical value.

2.1.4. Enrichment of the model

Combined mechanical and thermal loading. In the 1970s, Hart-Smith [16] enriched the 1D-bar model by considering a combined thermal and mechanical loading. In 1979, Chen and Nelson [17] provided a solution under the shear-lag approach of a three-layer assembly submitted to a pure thermal loading. The thermal expansion of adherends may lead to additional adhesive shear stress if these adherends have different thermal expansion coefficients. If adhesive thermal expansion is neglected and under uniform temperature variation Δ_T, the expression for the adhesive shear stress takes the following shape:

where α_i is the thermal expansion coefficient of the adherend i and $\xi\alpha = \alpha_2/\alpha_1$. This solution highlights the particular shapes of adhesive shear stress distribution. If both adherends are the same, then the adhesive shear stress distribution takes the shape of hyperbolic cosine. Moreover, the contribution due to the temperature variation vanishes. If the adherends are not the same, with or without temperature variation, the adhesive stress consists of a linear combination of hyperbolic cosine and hyperbolic sines. When the mechanical loading vanishes, only the hyperbolic sine component remains, ensuring an area under the adhesive shear stress distribution equal to zero.

Adherend shear stress. In 1998, Tsaï et al. [18] introduced in the 1D-bar model a linear variation of the shear stress through the adherend

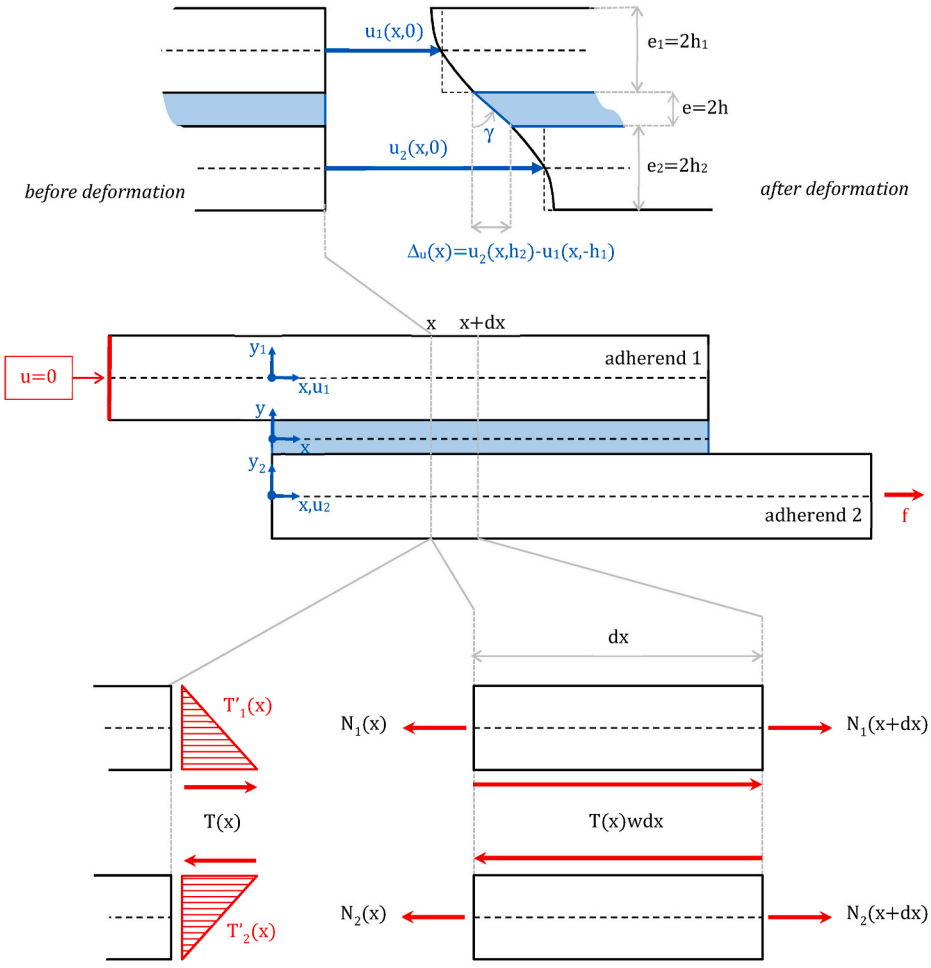

Fig. 6. Kinematics, parameterization and local equilibrium of the single-lap bonded joint under 1D-bar modelling with a linear shear stress through the adherend thickness.

thickness. The longitudinal displacement field is not constant through the thickness anymore, but rather parabolic (Fig. 6). The solution by Tsaï et al. is obtained from the that of Arnovljevic or Volkersen [4,5] by simply correcting the adhesive shear modulus value with a correction factor $1/(1+\kappa)$ such as:

$$G \rightarrow \frac{1}{1+\kappa} G \tag{20}$$

with:

$$\kappa = \frac{1}{3}\left(\frac{e_1}{G_1} + \frac{e_2}{G_2}\right) \tag{21}$$

Where G_i is the shear modulus of the adherend i. The adhesive shear stress then tends to be reduced compared to the initial shear-lag model (Fig. 5). The more the adhesive shear modulus is elevated, the more the reduction is significant. It should be noted that this simple modification can be applied to derive the related expressions for joint stiffness or adhesive shear stress under a combined mechanical and thermal loading. Besides, Demarkles [3] also assumed a linear variation of the shear stress through the thickness. The correction factor employed by Demarkles is $1/(1+3\kappa/2)$ instead of $1/(1+\kappa)$. On the one hand, Tsaï et al. computed the adherend normal force from a normal stress which is not constant through the adherend thickness, since it is obtained from the displacement field after integration of the adherend shear strain. On the other hand, Demarkles kept the normal stress as constant through the thickness leading to the difference between correction factors.

Based on Demarkles' approach, Adams and Pepiatt [10] considered the Poisson effect in the adherends on the adhesive shear stress and provided the expressions for the transverse shear stress induced by adherend Poisson strain. A closed-form solution is provided for a simplified governing set of ODEs, while it is indicated that a resolution scheme based on finite difference can be employed to solve the exact set of ODEs. Finally, Suhir [19–21] provided analytical formulae for the interface shear stress distribution of a multi-layered thermoset subjected to uniform temperature variation. The approach is based on the bimetal effect, for which the interface has it owns compliance, creating an additional normal strain at the interface dependent on the applied interface stress. The interface compliance is related to the Ribière solution for the longitudinal displacement field in a narrow strip subjected to a shear stress at the interface [22]; this solution is expanded in trigonometric series. In other words, the use of the Suhir approach allows for the inclusion of shear stress through the adherend thickness. When an adhesive layer owing its own interface compliance is taken into account, the shear correction factor is $1/(2/3+\kappa)$ [21].

2.1.5. Concluding remarks

The shear-lag model is likely not sufficiently complex to take into account the local behaviour of adherends and adhesive. The free edge of the adhesive layer is free from stress, so that the adhesive shear stress should vanish at both overlap ends instead of being the location of maximal stresses according to the 1D-bar analysis. The restrictions assumed on the stress tensors of adherends and of the adhesive do not allow for the representation of the physical stress state at both overlap ends [23,24]. These areas are subjected to high stress gradients, which promote the initiation then nucleation of micro-cracks and crack propagation. Moreover, according to Hart-Smith [16], the cohesive strength of the adhesive layer depends on its ability to deform by shearing. The choice of an elasto-plastic adhesive material would serve to increase the level of tensile flow to be transferred. In such a case, a nonlinear analysis associated with a dedicated resolution scheme could be more suitable. In addition, the strength of the adhesive layer is restricted by the presence of adhesive peeling stresses as shown by Hart-Smith [16,25]. The adhesive peeling stress arises from the eccentricity of the load path inducing the bending of adherends. To account for the peeling stress in the case of a single-lap joint under tension, in-plane and out-of-plane displacements must be introduced into the set of hypotheses.

2.2. More representative kinematics

2.2.1. Goland and Reissner's model

In 1944, Goland and Reissner [26] provided an analytical solution for the adhesive shear and peel stress along the overlap as well as a methodology for deriving the solution. In the case of relatively flexible joints, the hypotheses are as follows:

i. Quasi-static loading;
ii. Homogeneous linear elastic materials;
iii. The adherends are seen as Kirchhoff-Love plates undergoing cylindrical bending;
iv. The adhesive layer is seen as a homogeneous elastic foundation with two parameters associated with shearing and peeling, linking both adherend interfaces;
v. The geometrical parameters are constant.

Contrary to the shear-lag model, the adherends must be the same in terms of membrane and bending stiffnesses. Another limitation is that the joint has to be simply supported at both extremities, leading to a statically determinate configuration to solve (Fig. 7 and Fig. 8). Hereafter, we have chosen to explain the Goland and Reissner model by modifying the third hypothesis by "the adherends are seen as Euler-Bernoulli rectangular beams". This choice only implies (i) to consider the adherend bending stiffness $D_r = D_1 = D_2 = E_r e_r^3 w/12$ instead of $E_r e_r^3/12/(1-\nu_r^2)$, where E_r is the adherend Young's modulus, e_r is the adherend thickness and ν_r is the adherend Poisson's ratio and (ii) to work in force f instead of in flow $\varphi = f/w$. As a result, there is no loss of generalities.

The methodology presented by Goland and Reissner consists of a first step determining the shape of adhesive shear and peel stress as a function of integration constants by analysing the bonded overlap, termed sandwich, and of a second step assessing the integration constants according to the external load applied to the sandwich boundary (Fig. 7). Similarly to the shear-lag approach, the sandwich analysis starts with the constitutive equations and the local equilibrium equations of adherends. The governing system of equations then consists of twelve first-order ODEs and reads:

$$\begin{cases} \dfrac{dN_i}{dx} = (-1)^i w T \\ \dfrac{dV_i}{dx} = (-1)^{i+1} w S \\ \dfrac{dM_i}{dx} = -V_i - h_r w T \\ \dfrac{du_i}{dx} = \dfrac{N_i}{A_r} \\ \dfrac{dv_i}{dx} = \theta_i \\ \dfrac{d\theta_i}{dx} = \dfrac{M_i}{D_r} \end{cases} \quad i = 1,2 \tag{22a}$$

where S is the adhesive peeling stress, $h_1 = h_2 = h_r$ is the half thickness of the adherend, $A_1 = A_2 = A_r = E_r e_r w$ is the adherend membrane stiffness and v_i, θ_i, V_i and M_i are respectively the deflection, the bending angle, the shear force and the bending moment of the adherend i. Similarly to the shear-lag model, the adhesive stresses S and T allow for the coupling of the governing system of ODEs in Eq. (22); they are defined by:

$$\begin{cases} T = \dfrac{G}{e}(u_2 - u_1 - h_2\theta_2 - h_1\theta_1) \\ S = \dfrac{E}{e}(v_1 - v_2) \end{cases} \tag{23a}$$

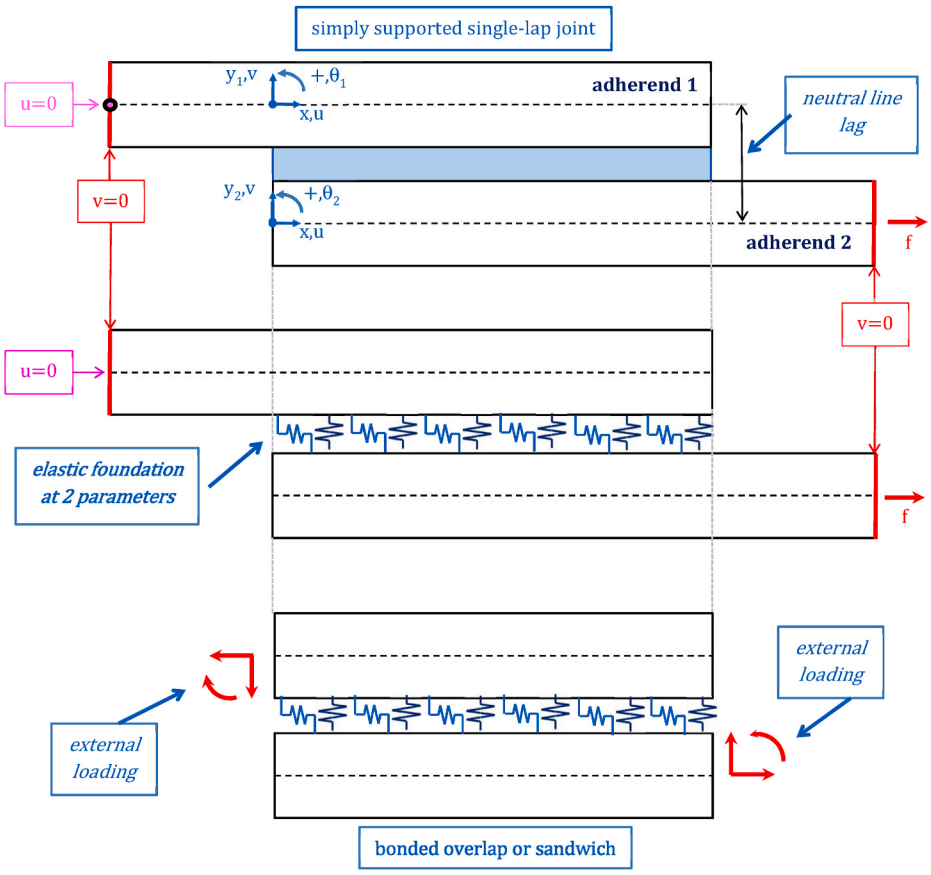

Fig. 7. Modelling principle of a single-lap bonded joint under in-plane and out-of-plane kinematics.

where E is the adhesive peel modulus. The adhesive may appear confined between two stiffer adherends. Hart-Smith suggests an assessment of the peel modulus which includes the transverse tensile stiffness of the adherends [16]. The use of the effective Young's modulus under one or two fixed strains is another approach to assess the peel modulus [27]. Besides, the mechanical state of the adhesive layer is spatially dependent [28]; along the free edges the adhesive layer is in a state of plane stress, while being in a plane strain state sufficiently far away from the edge.

Under the hypotheses set by Goland and Reissner, the manipulation of the governing system of ODEs leads to seven integration constants. These integration constants are then assessed by six equations expressed at overlap ends linking adhesive stresses and loads and 1 equation related to the load transfer through the adhesive layer. To determine the external loads applied to the sandwich, Goland and Reissner assumed that the flexibility of the adhesive layer can be neglected, so that the joint has a single variable cross-section and neutral line. Moreover, Goland and Reissner wrote the equilibrium of this beam in its deformed configuration to assess the internal loads. This leads to expressions of shear forces and bending moments at both sandwich ends, which depend non-linearly on the applied tensile load f. This non-linear dependency is included through a bending moment factor k_{GR} such as:

$$k_{GR} = \frac{1}{1 + 2\sqrt{2}\tanh\left(c\sqrt{\frac{f}{8D_r}}\right)} \tag{22b}$$

when the length of adherends outside the overlap is sufficiently large. The closed-form expression for the adhesive shear and peel stresses is then obtained under the following shape:

$$\begin{cases} T = \frac{1}{4}\left[3(1-k_{GR}) + \beta\frac{c}{e_r}(1+3k_{GR})\frac{\cosh\left(\frac{\beta c}{e_r}\left[\frac{x}{c}-1\right]\right)}{\sinh\left(\frac{\beta c}{e_r}\right)}\right]\left(\frac{f}{w2c}\right) \\ S = \left[\begin{array}{l}\left(\frac{1}{2}R_2\lambda k_{GR} + k'\cosh(\lambda)\cos(\lambda)\right)\cosh\left(\lambda\left[\frac{x}{c}-1\right]\right)\cos\left(\lambda\left[\frac{x}{c}-1\right]\right) \\ +\left(\frac{1}{2}R_1\lambda k_{GR} + k'\sinh(\lambda)\sin(\lambda)\right)\sinh\left(\lambda\left[\frac{x}{c}-1\right]\right)\sin\left(\lambda\left[\frac{x}{c}-1\right]\right)\end{array}\right]\frac{\lambda}{R_3}\left(\frac{e_r}{c}\right)^2\left(\frac{f}{we_r}\right) \end{cases} \tag{23b}$$

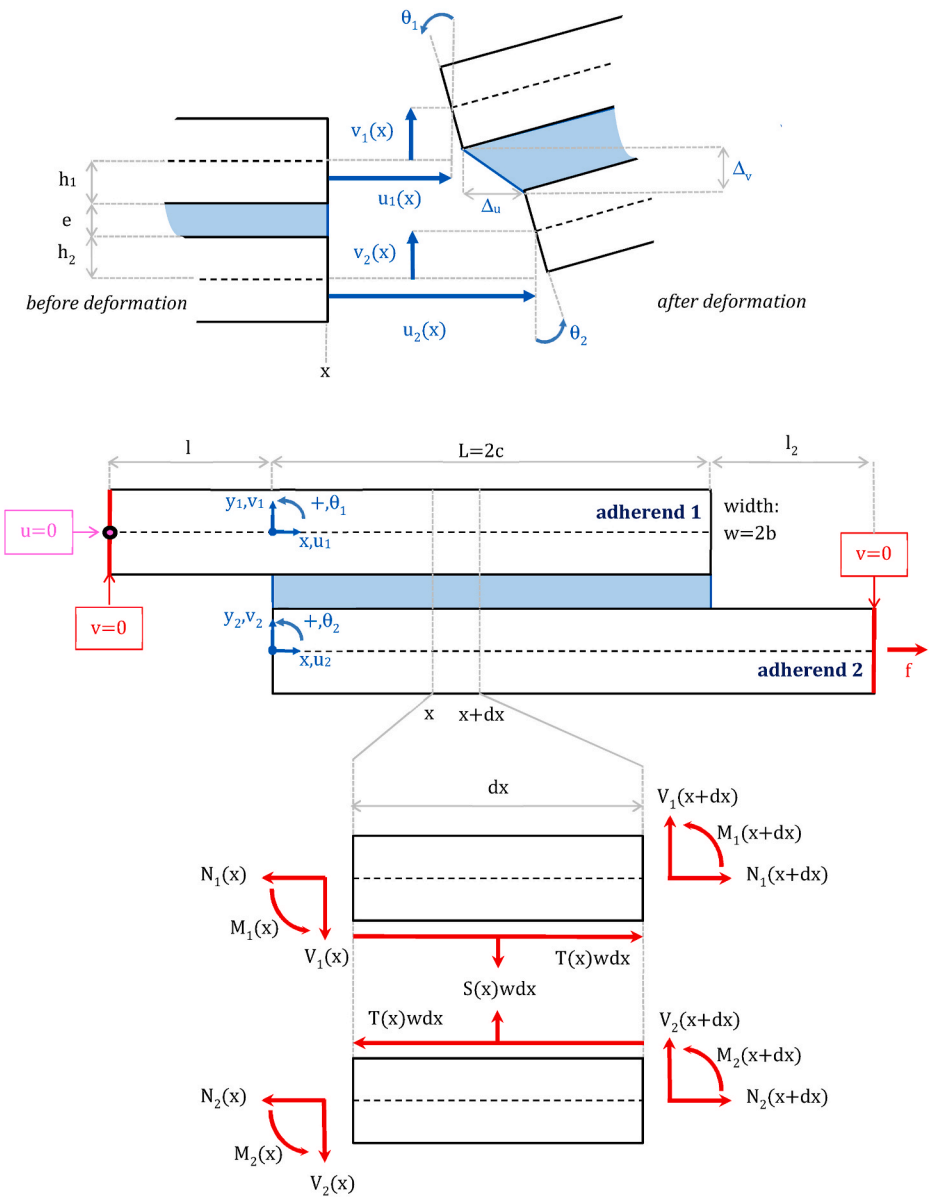

Fig. 8. Kinematics, parameterization and local equilibrium of the single-lap bonded joint following under in-plane and out-of-plane kinematics.

where:

$$\beta = \sqrt{8\frac{G}{E_r}\frac{e_r}{e}} \tag{24}$$

$$\lambda = \frac{c}{e_r}\sqrt[4]{6\frac{E}{E_r}\frac{e_r}{e}} \tag{25}$$

$$R_1 = \cosh(\lambda)\sin(\lambda) + \sinh(\lambda)\cos(\lambda) \tag{26}$$

$$R_2 = \sinh(\lambda)\cos(\lambda) - \cosh(\lambda)\sin(\lambda) \tag{27}$$

$$R_3 = \frac{1}{2}(\sinh(2\lambda) - \sin(2\lambda)) \tag{28}$$

$$k' = k_{GR}\frac{c}{e_r}\sqrt{3\frac{\varphi}{e_r E_r}} \tag{29}$$

An illustration of the distribution along the overlap of the adhesive shear and peel stress normalized by the normal tensile stress applied $\frac{f}{e_r w}$ is provided in Fig. 9. Elevated gradients of adhesive peel and shear stress are highlighted at both overlap ends. In addition to access to the adhesive peel stress, considering the bending tends to increase the shear stress concentration at both overlap ends. Consequently, it is deduced that the load appears to be transferred along a very small length at both overlap ends.

2.2.2. *Concluding remarks*

Like the shear-lag approach, the Goland and Reissner approach was improved to support a linear variation of shear stress through adherend thickness by Tsaï et al. [18]. Chen and Nelson [17] analysed a sandwich made of two dissimilar isotropic linear elastic adherends under cylindrical bending under a pure thermal load; this analysis makes use of the Goland and Reissner equilibrium. The solution is presented under closed-form but is not ready-to-use since the roots of the ODE characteristic equation are not explicitly given. The Suhir approach can be extended to the assessment of interface peel stress using dedicated interface compliances [29]. Zhang applied the Suhir approach to a three-layer model to take into account the thermal expansion of the adhesive layer [30]. Finally, the two-step methodology for the stress analysis presented by Goland and Reissner has subsequently been

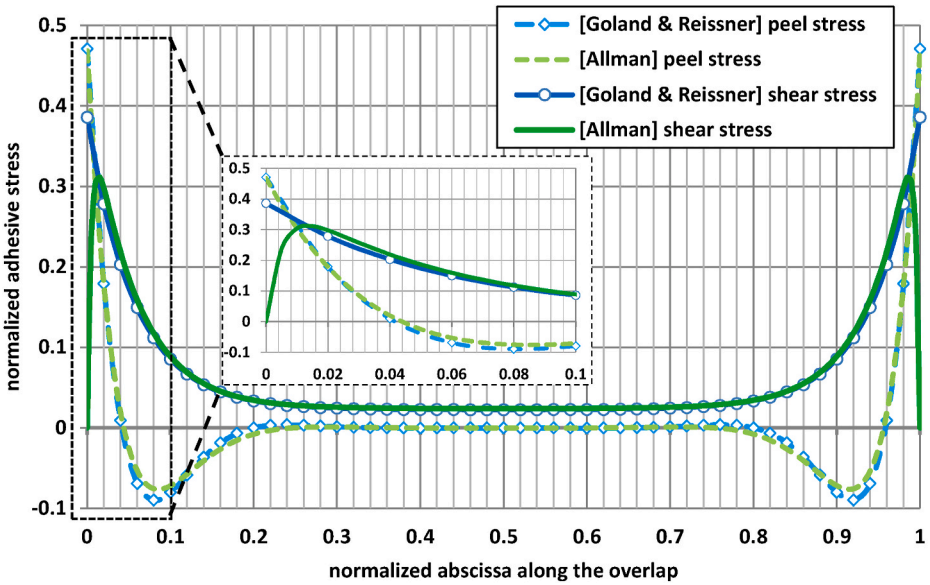

Fig. 9. Normalized adhesive stress as a function of the normalized abscissa along the overlap following the Goland and Reissner approach. Parameters used: $e_r = e_1 = e_2 = 1.6$ mm, $2c = w = 25$ mm, $E_r = E_1 = E_2 = 70$ GPa, $\nu_1 = \nu_2 = 0.33$, $E/e = 19280$ GPa mm^{-1}, $G/e = 6880$ MPa mm^{-1}, $f = 3.2$ kN.

applied by many authors.

3. Enrichment of fundamental theories including in- and out-of-plane displacements

The objective of this section is to highlight the restrictions to the scope of the closed-form solution when the set of simplifying hypotheses is less restrictive to be more representative of the physical reality. This section is based on existing theories in the literature. There is no attempt here to deliver an exhaustive literature review and the reader can refer to dedicated publications [31–35].

3.1. Beam or cylindrical bending plate on elastic foundation models

3.1.1. Analysis of the entire joint

For this section, the changes in terms of simplifying hypotheses compared to the Goland and Reissner model are highlighted. In the 1970s, Hart-Smith modified the linear elastic approach of Goland and Reissner by taking into account the adhesive thickness layer in the local equilibrium equation in moment [25]. Contrary to Goland and Reissner, both adherends are individually involved in the assessment of the bending moment factor allowing for the consideration of the adhesive layer shear strain. Moreover, a coefficient is introduced in the expression for the adherend bending stiffness to simply represent the eventual lamination of adherend materials. Closed-form solutions are obtained for the adhesive shear and peel stresses by neglecting the shear forces at both overlap ends, meaning that the area under the adhesive peel stress distribution along the overlap remains equal to zero. Finally, an elasto-plastic adhesive material behaviour is introduced and requires a semi-analytical resolution scheme. Ojalvo and Eidinoff [36] modified the Goland and Reissner model by considering that the adhesive longitudinal displacement and defection vary linearly through the adhesive thickness, while ensuring the compatibility of displacements at both interfaces. The presented model leads to a constant peel stress and a linear shear stress through the adhesive thickness. In particular, the adhesive shear stresses at both adhesive-to-adherend interfaces are not the same. A closed-form solution is provided for both the shear and peel stresses. In the 1990s, Oplinger [37,38] modified the Hart-Smith analysis by taking into account for the deflection of the overlap neutral line within the assessment of the overlap bending. The shape of the bending moment factor is significantly modified. In addition to the closed-form solution of the adhesive peel and shear stresses, a new expression for the bending moment factor is provided. In 1994, Tsaï and Morton [39] confronted the results from the closed-form solutions by Goland and Reissner, Hart-Smith and Oplinger with the results of geometrically non-linear dedicated FE models. It was shown that the bending moment factor by Hart-Smith (Oplinger) is the most suitable for shorter (larger) overlap lengths. In addition, they showed that the peel and shear stress distributions along the overlap given by Goland and Reissner remain in acceptable agreement for short and large overlap lengths. Between 2007 and 2009, Luo and Tong [40–42] chose a local equilibrium equation of adherend – modelled as Euler Bernoulli or Timoshenko laminated beams, possibly including the coupling bending membrane stiffness – which allows for the coupling of the bending moment with the normal forces. By construction, the governing ODEs tends to approximate the deformed configuration along the entire joint. For similar adherends, closed-form solutions for the adhesive peel and shear stresses are given. These solutions are closer to the results from a geometrically non-linear FE model than those by Goland and Reissner, Oplinger or Hart-Smith. In 2009, Wang and Zhang [43] published a three-parameter elastic foundation model allowing for the drop of adhesive shear stress to zero at both overlap ends. The adherends can be dissimilar and are modelled as Timoshenko isotropic beams. Contrary to the local equilibrium of adherends of Goland and Reissner, each of the adherends is subjected to a different peel stress at the adhesive interface. Three constitutive equations for the adhesive are then used: one for the shear stress and one for each of the peel stresses. These constitutive equations are compatible with the local equilibrium of the adhesive layer and induce the consideration of the adhesive shear force to ensure the global equilibrium of the joint. The external loads at the sandwich ends are computed as per Cheng et al. [44], who extended the Goland and Reissner assessment of the bending moment factor to the case where both adherends are dissimilar. The expressions for the adhesive shear and peel stresses are analytical but not ready-to-use. As such, a computer program is required to reach the results. It is shown that this model allows the adhesive shear stresses to vanish at both overlap ends.

3.1.2. Analysis of the sandwich

The determination of external loads at the sandwich may appear complicated and require the use of advanced numerical methods such as the FE method. Several authors have thus focused on the analysis of the sandwich, assuming the external loads to be known. In 1975, Williams

[45] provided a closed-form solution for the adhesive shear and peel stresses as a function of external loads at the sandwich end considering the Goland and Reissner sandwich with two dissimilar Euler-Bernoulli isotropic beams. In 1977, Renton and Vinson [46] assumed two dissimilar laminated adherends in plane strain and including shear and normal strain through the thickness, along with thermal expansion. In particular, a parabolic variation of the adherend shear stress is assumed. The resolution scheme is semi-analytical and leads to adhesive shear stress vanishing at both overlap ends. In 1981, Delale et al. [47] considered two dissimilar adherends, possibly laminated and considered as Mindlin Reissner plates. The adhesive longitudinal strains were considered from the average of adherend longitudinal strains at the interfaces and introduced in the peel strain thanks to the Poisson effect. The local equilibrium of Hart-Smith was applied. A closed-form solution was provided according to the external loads at the sandwich ends. In 1989, Bigwood and Crocombe [48] provided the expressions for maximal adhesive shear and peel stresses as a function of external loads at the sandwich ends made of dissimilar adherends and using the Hart-Smith local equilibrium. In 1990, Bigwood and Crocombe [49] used a finite difference scheme to numerically solve the set of nonlinear equations, assuming the adhesive material to have a nonlinear behaviour. From 2004, Högberg [50] then Alfredsson and Högberg [51] provided a closed-from solution of adhesive peel and shear stress distributions as a function of the conditions at the sandwich ends expressed in terms of displacement or loads. In their analysis, the adherends were dissimilar and seen as Euler-Bernoulli isotropic beams and the Goland and Reissner local equilibrium was used. In 2014, Weiβgraeber et al. [52] presented a semi-analytical resolution for the adhesive peel and shear stress distributions. The adherends were seen as Mindlin-Reissner laminated plates including the coupling membrane bending stiffness. The local equilibrium of adherends according to Hart-Smith was chosen. The same year, a semi-analytical resolution was provided by Liu et al. [53] as function of displacement or loads applied at sandwich ends. The adherends were dissimilar and modelled as Timoshenko laminated beams including the coupling membrane bending stiffness under the Goland and Reissner local equilibrium.

3.2. *Plane continuum media models*

The second category of simplified analysis of single-lap bonded joints consists of plane continuum media models. Allman [54] and Chen and Cheng [55] added the local equilibrium of the adhesive to the local equilibrium of adherends. It is assumed that the shear stress remains constant through the adhesive thickness. The application of local equilibrium equation in conjunction with constant adhesive shear stress through the thickness leads to a linear variation of the adhesive peel stress through the thickness and a normal adhesive stress equal to zero along the entire overlap. Consequently, the slope of the adhesive shear stress with respect to the overlap length coordinate is equal to the ratio between the differences between both peel stresses acting on the adherends at the interface divided by the thickness of the adhesive layer. Moreover, the normal stress is assumed to vary linearly through the adherend thickness and the stresses are continuous at both adherend-to-adhesive interfaces. The stress state in the adherends can then be expressed as functions of adhesive stresses at the interface and of adherend internal load making use of the local equilibrium equations of Goland and Reissner. Closed-form solutions in the form of ready-to-use equations are provided for the case of the single-lap bonded joint where (i) the adherends are similar and (ii) the external loads at the sandwich ends are those of Goland and Reissner. To support various geometrical and material conditions, a dedicated numerical resolution scheme is required, whose presentation is referred to in RAE Tech Report no. 76024. According to the Allman model, it is found that the adhesive shear stresses at both overlap ends vanish. A comparison of adhesive peel and shear stress distributions along the overlap according to the Goland and Reissner theory and the Allman theory is provided in Fig. 9. It is shown that both adhesive peel stress distributions are very close each other. Moreover, it is obvious that the adhesive shear stress peaks cannot occur at the same location along the overlap. The drop to zero stress is characterized by an elevated gradient, so that the peak is slightly shifted within the overlap. Finally, both values of adhesive shear stress peaks appear as different, considering that the area under the adhesive shear stress distribution is set to the applied tensile flow. In 1992, Adams and Mallick [56] developed a model under plane stress or plane strain for which the adhesive and adherend normal stresses vary linearly through the thickness. The adhesive shear stress is thus no longer constant through the thickness. According to Allman, the integration of local equilibrium equations associated with the continuity of stresses at the adherend-to-adhesive interfaces is performed thanks to a dedicated numerical scheme inspired by the FE method and based on a meshing. The resolution scheme developed can be introduced into an iterative procedure with consideration of nonlinear adhesive material. In 2010, Nemes and Lachaud [57] focused on the case of a symmetrical double joint neglecting the out-of-plane displacement under plane stress state. The adhesive normal stress is assumed to vanish at every point. It is imposed that the adhesive and adherend stresses are such as the local equilibrium equations, the free edge conditions and continuity at the adherend-to-adhesive interface. Application of the complementary strain-energy theorem leads to the resolution of a unique fourth-order linear ODE whose solution is not provided in closed-form. In 2012, Chen and Qiao [58] modelled the adherends as Timoshenko beams and the adhesive as a simplified plane continuum medium. It is assumed that the adhesive normal displacement varies linearly through the thickness similarly to a beam model; it is defined from the normal displacement along the adhesive neutral line and the first derivative of the transverse displacement, assumed to be dependent on the overlap length coordinate only. The Poisson effect is then neglected. According to Suhir, interface compliances are used to write the continuity of displacements at both adherend-to-adhesive interfaces. An eighth-order linear ODE is then obtained associated with eight boundary conditions expressed in terms of internal loads. The roots and integration constants are not determined in closed-form manner. Jiang and Qiao [59] in 2015 and Du et al. [60] in 2019, improved the Chen and Qiao model by assuming that the transverse displacement of the adhesive neutral line is equal to the average over the adhesive thickness of transverse displacement. The solution is not provided in the form of ready-to-use equations. In 2021, Nguyen and Le Grognec [61] enhanced the previous approaches by starting from the enrichment of the kinematics within the adhesive layer in order to describe the longitudinal stress and its variations along both the length and through the thickness of the adhesive joint. So, the adherends are represented by Timoshenko beams, and the adhesive layer is defined as a 2D continuous medium with polynomial dependence of the displacement fields with respect to the thickness. According to the polynomial degree and considering dissimilar adherents, the shear stress can drop to zero at both overlap ends. The solution is not however provided in the form of ready-to-use equations. Finally, it is indicated that some authors attempted to provide approximated – instead of exact – closed-form solutions using resolution schemes based on Fourier expansion series or Taylor expansion power series (TEPS) such as those published in Refs. [62–64] for example. The resulting equations are then not ready-to-use. Gilibert and Rigolot [23,24] analysed the mechanical behaviour of a symmetrical double-lap bonded joint using an approach based on asymptotic expansion-based analysis of the adhesive and adherend regarded as elastic continuum media. In such a configuration, it is often assumed that the adhesive stress tensor components van be neglected compared to the in-plane shear stress component according to the Arnovljevic or Volkersen [4,5] model. Using an approach based on asymptotical expansions, Gilibert and Rigolot showed that this assumption makes sense on a large length of the overlap, while a boundary layer effect is highlighted close to the adhesive free edges. In this boundary layer, adhesive longitudinal and peeling stresses exist and exhibit elevated gradients. Closed-form ready-to-use equations are

provided for the adhesive stress distributions. This boundary layer effect was also shown by Radice in 2018 [65] through a model – called Decoupled Biharmonic model – and focusing on the adhesive layer subjected to traction free surfaces and imposed displacement boundary conditions. The approach is comprehensively described and asymptotically satisfied the biharmonic Airy function. The solution is not given in the form of closed-form ready-to-use equations and an eight by eight linear system must be inverted. Finally, the previous models assume an adhesive square end surface over which the traction free conditions are applied. It is noteworthy that this ideal condition is difficult to produce in real life and a spew fillet, whose shape may be controlled or not, is likely present. The presence of spew fillets could lead to an increase in the strength of the bonded joints by reducing the amount of stress singularities at the interfaces with the adherends [66,67]. When the adhesive material is assumed to be elasto-plastic, the ability to accommodate the stress by its deformability drives the strength of the joint since the stress peaks are clipped and the load transfer is redistributed along the overlap [16,68].

3.3. Concluding remarks

While numerous works have been published since Goland and Reissner, the scope of closed-form and ready-to-use solutions is restricted. The applications of boundary conditions and the nature of the materials to be joined are both difficulties to address when the materials are assumed to have a linear elastic behaviour. Dedicated resolution schemes are then used to overcome these difficulties applied to a particular set of simplifying hypotheses. At the end of the 1990s Mortensen and Thomsen [69–72] provided a semi-analytical approach allowing for extension of the scope of the first family of models (adherends on elastic foundation) by supporting various boundary conditions, loadings and geometries. The adherends are linear elastic and are seen as Euler-Bernoulli laminated beams or Kirchhoff-Love laminated plates under cylindrical bending, including the Poisson effect. The adhesive layer is an elastic foundation involving peel and both shear deformation modes and possibly with nonlinear behaviours. The resolution scheme is based on the multi-segment method of integration [73].

4. Macro-element modelling

4.1. Overview

Macro-element (ME) modelling has been developed since 2004 for the simplified stress analysis of HBB joints [74–81]. Applied to pure bonded joints, ME modelling is a semi-analytical method extending the scope of models belonging to the first family. It offers the advantage of providing a solution for geometrical, material and loading configurations for which there are no closed-form solutions [81–93]. As demonstrated in sections 4 and 5, ME modelling is an attractive approach to support the variation and associated growing complexity of simplifying hypotheses at low computational cost. In particular, the ME modelling is able to support various in-plane force and/or displacement loadings, including statically indeterminate ones. A ME is a 4-node brick integrating the assumed physics of the adherends and the adhesive in terms of constitutive and local equilibrium equations. Compared to the standard FE method, ME modelling differs by the formulation methodologies involved allowing for model enrichment. To reduce the size of FE models, 2D plane stress or strain or 3D special FEs were developed and published. These special FEs could represent the adhesive layer [94–99] or the adhesive and the adherends [100–104]. These special FEs make use of assumed shape functions, such that meshing is required to approximate the solution. Contrary to the special FEs and as seen in section 4, the ME stiffness matrix does not make use of assumed shape functions, so that a single ME is able to model an entire overlap. Like standard FEs or special FEs, a ME is represented by a stiffness matrix linking the nodal forces to the nodal displacements. Finally, over the same period of time and independently of ME modelling, a *joint element* was developed to model the adherends and adhesive within a single brick and again without hypotheses on shape function [105–111].

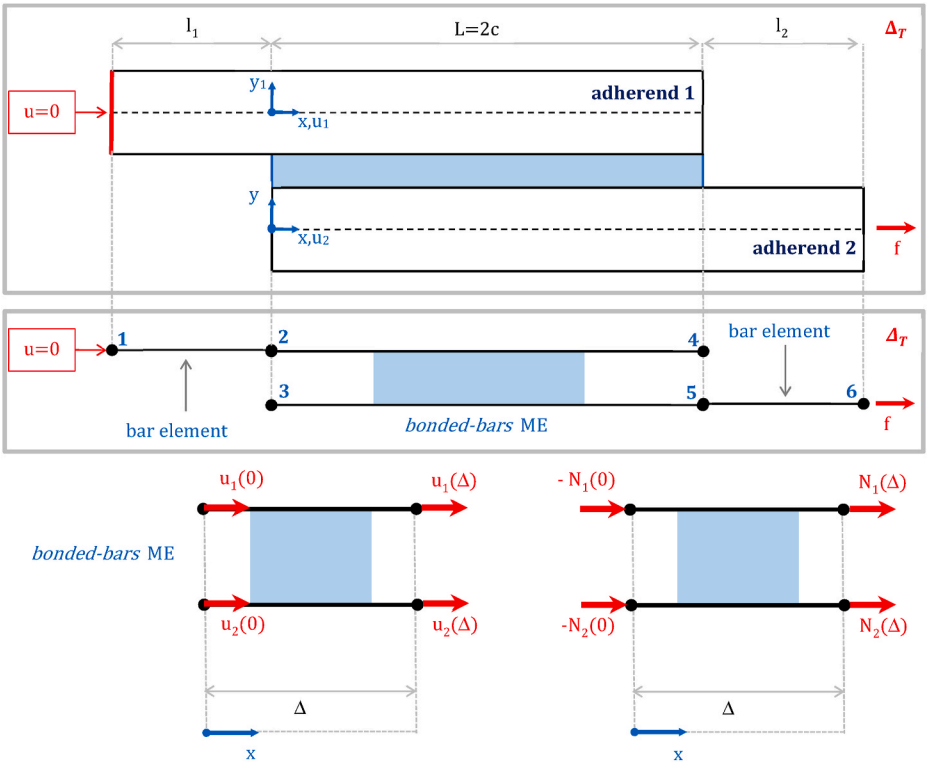

Fig. 10. 1D-bar ME model of a single-lap bonded joint.

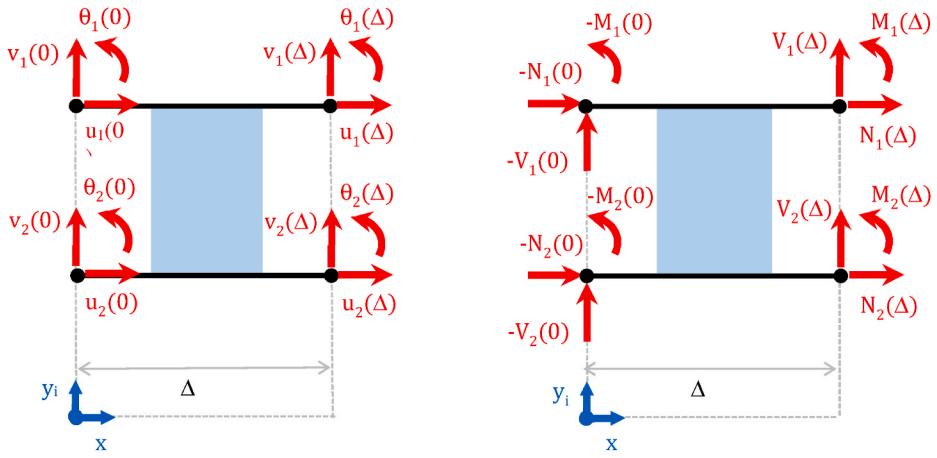

Fig. 11. Nodal displacements and forces associated with the bonded-beams ME.

4.2. Shear-lag approach

4.2.1. Method description

The objective of this section is to explain ME modelling based on the simple frame of 1D-bar analysis. ME modelling consists firstly in discretizing the single-lap bonded joints with 1 bar elements for each adherend outside the overlap and one *bonded-bars* ME for the sandwich (see Fig. 10). The model then consists of a total of six nodes and 6° of freedom (DoF) since each node counts one DoF per node. From the elementary stiffness matrices, the stiffness matrix of the entire joint denoted K_s is assembled. Accounting for the boundary conditions, the longitudinal displacement of node 1 is prescribed and the tensile force f is applied to node 6, leading to the nodal force and displacement vectors quoted F_s and U_s respectively. Minimization of the potential energy requires the linear system $F_s = K_s U_s$ to be solved. The elementary stiffness matrix K_e of the bonded-bars ME must then be formulated. Contrary to the FE method, the shape of ME shape functions is not assumed a priori. These functions take the shape of the solution shape of the system of governing coupled ODEs. From the computation of U_s by solving the five-by-five linear system $F_s = K_s U_s$, it is then possible to identify the integration constants and to assess the expressions for the adherend longitudinal displacements and normal forces, along with the adhesive shear stress at any point of the single-lap joint (see Fig. 11).

4.2.2. Formulation ME elementary stiffness matrix

The formulation of the elementary stiffness matrix of the bonded-bars ME is based on the same set as the Arnovjlevic or Volkersen model [4,5] (see section 2.1.1). The aim is to determine the linear relationships between the elementary nodal displacement vector U_e and the elementary nodal force vector F_e such that $F_e = K_e U_e$. Using Eqs (3), (5) and (6), the longitudinal displacements can be written as:

$$\begin{pmatrix} u_1 \\ u_2 \end{pmatrix} = \frac{1}{2}\begin{pmatrix} 1 & x & -\frac{2\xi}{1+\xi}e^{-\eta x} & -\frac{2\xi}{1+\xi}e^{\eta x} \\ 1 & x & \frac{2}{1+\xi}e^{-\eta x} & \frac{2}{1+\xi}e^{\eta x} \end{pmatrix} C \tag{30}$$

where:

$$C = \begin{pmatrix} c_1 \\ c_2 \\ c_3 \\ c_4 \end{pmatrix} \tag{31}$$

From these previous expressions for the adherend longitudinal displacements and the adherend constitutive equations in Eq. (1), two coupling matrices ${D_e}^{-1}$ and L_e are written in closed-form:

$$C = \boldsymbol{D_e}^{-1}\boldsymbol{U_e} \Leftrightarrow \boldsymbol{C} = \begin{pmatrix} \frac{2}{1+\xi} & \frac{2\xi}{1+\xi} & 0 & 0 \\ -\frac{2}{(1+\xi)\Delta} & -\frac{2\xi}{(1+\xi)\Delta} & \frac{2}{(1+\xi)\Delta} & \frac{2\xi}{(1+\xi)\Delta} \\ -\frac{e^{\eta\Delta}}{2\sinh\eta\Delta} & \frac{e^{\eta\Delta}}{2\sinh\eta\Delta} & \frac{1}{2\sinh\eta\Delta} & -\frac{1}{2\sinh\eta\Delta} \\ \frac{e^{-\eta\Delta}}{2\sinh\eta\Delta} & -\frac{e^{\eta-\Delta}}{2\sinh\eta\Delta} & -\frac{1}{2\sinh\eta\Delta} & \frac{1}{2\sinh\eta\Delta} \end{pmatrix} \begin{pmatrix} \boldsymbol{u}_1(0) \\ \boldsymbol{u}_2(0) \\ \boldsymbol{u}_1(\Delta) \\ \boldsymbol{u}_2(\Delta) \end{pmatrix} \tag{32}$$

$$\boldsymbol{F_e} = \boldsymbol{L_e}\boldsymbol{C} \Leftrightarrow \begin{pmatrix} -\boldsymbol{N}_1(0) \\ -\boldsymbol{N}_2(0) \\ \boldsymbol{N}_1(\Delta) \\ \boldsymbol{N}_2(\Delta) \end{pmatrix} = \frac{1}{2}\begin{pmatrix} 0 & -\boldsymbol{A}_1 & -\eta\frac{2\xi}{1+\xi}\boldsymbol{A}_1 & \eta\frac{2\xi}{1+\xi}\boldsymbol{A}_1 \\ 0 & -\boldsymbol{A}_2 & \eta\frac{2}{1+\xi}\boldsymbol{A}_2 & -\eta\frac{2}{1+\xi}\boldsymbol{A}_2 \\ 0 & \boldsymbol{A}_1 & \eta\frac{2\xi}{1+\xi}e^{-\eta\Delta}\boldsymbol{A}_1 & -\eta\frac{2\xi}{1+\xi}e^{\eta\Delta}\boldsymbol{A}_1 \\ 0 & \boldsymbol{A}_2 & -\eta\frac{2}{1+\xi}e^{-\eta\Delta}\boldsymbol{A}_2 & \eta\frac{2}{1+\xi}e^{\eta\Delta}\boldsymbol{A}_2 \end{pmatrix} \boldsymbol{C} \tag{33}$$

where Δ is the length of the ME. The elementary stiffness matrix for the bonded-bars ME is then obtained in closed-form by a simple matrix product:

$$\boldsymbol{K}_e = \boldsymbol{L}_e \boldsymbol{D}_e^{-1} = \frac{1}{1+\xi}\frac{\boldsymbol{A}_2}{\Delta}\begin{pmatrix} \frac{\eta\Delta}{\tanh\eta\Delta}+\frac{1}{\xi} & 1-\frac{\eta\Delta}{\tanh\eta\Delta} & -\frac{\eta\Delta}{\sinh\eta\Delta}-\frac{1}{\xi} & \frac{\eta\Delta}{\sinh\eta\Delta}-1 \\ 1-\frac{\eta\Delta}{\tanh\eta\Delta} & \frac{\eta\Delta}{\tanh\eta\Delta}+\xi & \frac{\eta\Delta}{\sinh\eta\Delta}-1 & -\frac{\eta\Delta}{\sinh\eta\Delta}-\xi \\ -\frac{\eta\Delta}{\sinh\eta\Delta}-\frac{1}{\xi} & \frac{\eta\Delta}{\sinh\eta\Delta}-1 & \frac{\eta\Delta}{\tanh\eta\Delta}+\frac{1}{\xi} & 1-\frac{\eta\Delta}{\tanh\eta\Delta} \\ \frac{\eta\Delta}{\sinh\eta\Delta}-1 & -\frac{\eta\Delta}{\sinh\eta\Delta}-\xi & 1-\frac{\eta\Delta}{\tanh\eta\Delta} & \frac{\eta\Delta}{\tanh\eta\Delta}+\xi \end{pmatrix} \tag{34}$$

4.2.3. Resolution

In addition to mechanical loading, a uniform temperature variation Δ_T is applied such as in the model by Hart-Smith [16] (see section 2.1.4). The stiffness matrix of bar elements is in the following form:

$$\boldsymbol{K}_{bar,i} = \frac{\boldsymbol{A}_i}{\boldsymbol{l}_i}\begin{pmatrix} 1 & -1 \\ -1 & 1 \end{pmatrix} \quad \boldsymbol{i} = 1,2 \tag{35}$$

By adding the loads equivalent to the thermal loading to the nodal force vector, the linear system to be solved is written as follows:

$$\boldsymbol{F}_s = \boldsymbol{K}_s \boldsymbol{U}_s \Leftrightarrow \begin{pmatrix} 0 \\ -\boldsymbol{A}_2\boldsymbol{\alpha}_2\Delta_T \\ \boldsymbol{A}_1\boldsymbol{\alpha}_1\Delta_T \\ 0 \\ \boldsymbol{f}+\boldsymbol{A}_2\boldsymbol{\alpha}_2\Delta_T \end{pmatrix} = \boldsymbol{K}_s \begin{pmatrix} \boldsymbol{u}_{[2]} \\ \boldsymbol{u}_{[3]} \\ \boldsymbol{u}_{[4]} \\ \boldsymbol{u}_{[5]} \\ \boldsymbol{u}_{[6]} \end{pmatrix} \tag{36}$$

where:

$$\boldsymbol{K}_s = \frac{1}{1+\xi}\frac{\boldsymbol{A}_2}{\boldsymbol{L}}\begin{pmatrix} \frac{\eta\boldsymbol{L}}{\tanh\eta\boldsymbol{L}}+\frac{1}{\xi}+\frac{1+\xi}{\xi}\frac{\boldsymbol{L}}{\boldsymbol{l}_1} & 1-\frac{\eta\boldsymbol{L}}{\tanh\eta\boldsymbol{L}} & -\frac{\eta\boldsymbol{L}}{\sinh\eta\boldsymbol{L}}-\frac{1}{\xi} & \frac{\eta\boldsymbol{L}}{\sinh\eta\boldsymbol{L}}-1 & 0 \\ 1-\frac{\eta\boldsymbol{L}}{\tanh\eta\boldsymbol{L}} & \frac{\eta\boldsymbol{L}}{\tanh\eta\boldsymbol{L}}+\xi & \frac{\eta\boldsymbol{L}}{\sinh\eta\boldsymbol{L}}-1 & -\frac{\eta\boldsymbol{L}}{\sinh\eta\boldsymbol{L}}-\xi & 0 \\ -\frac{\eta\boldsymbol{L}}{\sinh\eta\boldsymbol{L}}-\frac{1}{\xi} & \frac{\eta\boldsymbol{L}}{\sinh\eta\boldsymbol{L}}-1 & \frac{\eta\boldsymbol{L}}{\tanh\eta\boldsymbol{L}}+\frac{1}{\xi} & 1-\frac{\eta\boldsymbol{L}}{\tanh\eta\boldsymbol{L}} & 0 \\ \frac{\eta\boldsymbol{L}}{\sinh\eta\boldsymbol{L}}-1 & -\frac{\eta\boldsymbol{L}}{\sinh\eta\boldsymbol{L}}-\xi & 1-\frac{\eta\boldsymbol{L}}{\tanh\eta\boldsymbol{L}} & \frac{\eta\boldsymbol{L}}{\tanh\eta\boldsymbol{L}}+\xi+(1+\xi)\frac{\boldsymbol{L}}{\boldsymbol{l}_2} & -(1+\xi)\frac{\boldsymbol{L}}{\boldsymbol{l}_2} \\ 0 & 0 & 0 & -(1+\xi)\frac{\boldsymbol{L}}{\boldsymbol{l}_2} & (1+\xi)\frac{\boldsymbol{L}}{\boldsymbol{l}_2} \end{pmatrix} \tag{37}$$

and $u_{[i]}$ is the nodal displacement of the node i. ME modelling takes then advantage of the flexibility and efficiency of the FE method. In particular, any kind of loadings can be easily introduced, including those related to statically indeterminate configurations. The vector of integration constants is not expressed in closed-form. It is computed only when the nodal displacements are computed in order to assess the adherend longitudinal displacement and normal forces, as the adhesive shear stress as well as the stiffness of the entire joint or of the overlap. It is not worth saying that a linear variation of the adherend shear stress through the thickness following Tsaï et al. [18] can enrich the ME by simply adapting the adhesive shear modulus according to section 2.1.4. Finally, in the context of the shear-lag approach, the use of ME modelling does not seem relevant in the case on an elastic linear analysis due to the existence of closed-form and ready-to-use equations. Nevertheless, it can be of use in the analysis of more complex configurations such as nonlinear material behaviours, geometrical and/or mechanical properties graduation, multiple-lap joints or HBB joints [74,76,80,82,83,90,91].

4.3. Beam or cylindrical bending plate

The consideration of in- and out-of-plane displacement, which is more representative for the mechanical behaviour of a single-lap joint, highlights the benefits of ME modelling. This section concerns the methodologies developed to formulate the elementary stiffness matrix of the *bonded-beams* ME. It is indicated that the aim of this review paper is not to provide the mathematical details, which can be found in the related papers.

4.3.1. Initial methodology

The first formulation of the elementary stiffness matrix of the *bonded-beams* ME provided in Refs. [74,75,77] assumed two similar linear elastic adherends. The formulation for the *bonded-beams* ME with dissimilar laminated adherends was published from 2011 [79,81–85]. The initial methodology employed for the formulation focuses on closed-form equations, as for the *bonded-bars* ME. The key point of this methodology is the ability to write the expressions for adhesive shear (T) and peel (S) stress. However, contrary to the shear-lag approach and considering the literature review given in section 3, the components of the elementary stiffness matrix cannot be provided in closed-form expression. The simplifying hypotheses taken are those of Goland and Reissner (see section 2.2.1), except for the adherend constitutive relationships, which are regarded as Euler-Bernoulli laminated beams including the coupling membrane-bending stiffness. The governing system of ODEs is then composed of twelve coupled linear first order ODEs:

$$\begin{cases} \dfrac{dN_i}{dx} = (-1)^i \boldsymbol{wT} \\ \dfrac{dV_i}{dx} = (-1)^{i+1} \boldsymbol{wS} \\ \dfrac{dM_i}{dx} = -V_i - h_i \boldsymbol{wT} \\ \dfrac{du_i}{dx} = \dfrac{D_i}{\Delta_i} N_i + \dfrac{B_i}{\Delta_i} M_i \\ \dfrac{dv_i}{dx} = \theta_i \\ \dfrac{d\theta_i}{dx} = \dfrac{B_i}{\Delta_i} N_i + \dfrac{A_i}{\Delta_i} M_i \end{cases} \quad i = 1,2 \tag{37a}$$

where, for the adherend i, D_i is the bending stiffness, B_i is the coupling membrane-bending stiffness, hi is the half-thickness and $\Delta_i = A_i D_i - B_i B_i \neq 0$. When both adherends are assumed to be dissimilar, the coupling between ODEs is increased, such that the system of ODEs in T and S reads:

$$\begin{cases} \dfrac{d^3 \boldsymbol{T}}{dx^3} = k_1 \dfrac{d\boldsymbol{T}}{dx} + k_2 \boldsymbol{S} \\ \dfrac{d^4 \boldsymbol{S}}{dx^4} = -k_3 \dfrac{d\boldsymbol{T}}{dx} - k_4 \boldsymbol{S} \end{cases} \tag{38}$$

where:

$$\begin{cases} k_1 = w \dfrac{G}{e} \left[\dfrac{D_1}{\Delta_1} \left(1 + \dfrac{{h_1}^2 A_1}{D_1} \right) + \dfrac{D_2}{\Delta_2} \left(1 + \dfrac{{h_2}^2 A_2}{D_2} \right) + 2 \left(\dfrac{h_1 B_1}{\Delta_1} - \dfrac{h_2 B_2}{\Delta_2} \right) \right] \\ k_2 = w \dfrac{G}{e} \left[\dfrac{h_1 A_1}{\Delta_1} - \dfrac{h_2 A_2}{\Delta_2} + \left(\dfrac{B_1}{\Delta_1} + \dfrac{B_2}{\Delta_2} \right) \right] \\ k_3 = w \dfrac{E}{e} \left[\dfrac{h_1 A_1}{\Delta_1} - \dfrac{h_2 A_2}{\Delta_2} + \left(\dfrac{B_1}{\Delta_1} + \dfrac{B_2}{\Delta_2} \right) \right] \\ k_4 = w \dfrac{E}{e} \left[\dfrac{A_1}{\Delta_1} + \dfrac{A_2}{\Delta_2} \right] \end{cases} \tag{39}$$

Under the hypotheses of Goland and Reissner, the parameters k_2 and k_3 vanish such that the ODEs in T and S are naturally uncoupled. The uncoupling of the governing system of ODEs in Eq (38) requires several manipulations associated with an increase in ODE order leading to:

$$\begin{cases} \dfrac{d^6 \boldsymbol{S}}{dx^6} - k_1 \dfrac{d^4 \boldsymbol{S}}{dx^4} + k_4 \dfrac{d^2 \boldsymbol{S}}{dx^2} + (k_2 k_3 - k_1 k_4) \boldsymbol{S} = 0 \\ \dfrac{d}{dx} \left[\dfrac{d^6 \boldsymbol{T}}{dx^6} - k_1 \dfrac{d^4 \boldsymbol{T}}{dx^4} + k_4 \dfrac{d^2 \boldsymbol{T}}{dx^2} + (k_2 k_3 - k_1 k_4) \boldsymbol{T} \right] = 0 \end{cases} \tag{40}$$

The first derivatives of T and S are then the solution of linear sixth order ODEs, which has the particularity of being bi-squared. It is then possible to obtain the closed-form equations of eigenvalues using the Cardano's method for the assessment of roots of third order polynomial expressions. Depending on the Cardano's discriminant, there are at least four possible sets of eigenvalues [85] leading to four different shapes of solutions for S and T:

$$\begin{cases} T(x) = K_1 e^{sx} \sin tx + K_2 e^{sx} \cos tx + K_3 e^{-sx} \sin tx + K_4 e^{-sx} \cos tx + K_5 e^{rx} + K_6 e^{-rx} + K_7 \\ S(x) = K_8 e^{sx} \sin tx + K_9 e^{sx} \cos tx + K_{10} e^{-sx} \sin tx + K_{11} e^{-sx} \cos tx + K_{12} e^{rx} + K_{13} e^{-rx} \end{cases} \tag{40a}$$

$$\begin{cases} T(x) = K_1 e^{sx} \sin tx + K_2 e^{sx} \cos tx + K_3 e^{-sx} \sin tx + K_4 e^{-sx} \cos tx + K_5 \sin rx + K_6 \cos rx + K_7 \\ S(x) = K_8 e^{sx} \sin tx + K_9 e^{sx} \cos tx + K_{10} e^{-sx} \sin tx + K_{11} e^{-sx} \cos tx + K_{12} \sin rx + K_{13} \cos rx \end{cases} \tag{41}$$

$$\begin{cases} T(x) = K_1 \sin t'x + K_2 \cos t'x + K_3 \sin s'x + K_4 \cos s'x + K_5 e^{r'x} + K_6 e^{-r'x} + K_7 \\ S(x) = K_8 \sin t'x + K_9 \cos t'x + K_{10} \sin s'x + K_{11} \cos s'x + K_{12} e^{r'x} + K_{13} e^{-r'x} \end{cases} \tag{42}$$

$$\begin{cases} T(x) = K_1 \sin t'x + K_2 \cos t'x + K_3 e^{s'x} + K_4 e^{-s'x} + K_5 e^{r'x} + K_6 e^{-r'x} + K_7 \\ S(x) = K_8 \sin t'x + K_9 \cos t'x + K_{10} e^{s'x} + K_{11} e^{-s'x} + K_{12} e^{r'x} + K_{13} e^{-r'x} \end{cases} \tag{43}$$

where K_i are the thirteen integration constants and r, r', s, s', t and t' real numbers. The solutions for T and S given in Eq. (40) are the solutions to be considered for all geometrical and material parameters having a physical meaning [45,50] when the adherends are dissimilar and $B_1 = B_2 = 0$. The adherend displacements and internal forces can be written as functions of the expressions for adhesive stresses and their derivatives as well as polynomial expressions [79,81–85]. In addition to the first thirteen integration constants K_1 to K_{13}, fourteen new integration constants appear. The *bonded-beams* ME, however, has 3 DoFs for each of 4 nodes (Fig. 9). As a result, as set of twelve integration constants must be identified. The identification is performed by introducing the deduced closed-form expressions for adherend displacements, internal loads and adhesive stresses in Eq. (38) and particular governing ODEs following Högberg [50]. Once the twelve integration constants have identified the coupling matrices ${D_e}^{-1}$ and L_e, then the elementary stiffness matrix $K_e = L_e {D_e}^{-1}$ can be assessed. At this stage, a computer code is required to assess the components of the previous matrices. It has been shown in Refs. [79,81–85] that the stiffness matrix of beam elements representing the adherend outside the overlap takes the following shape:

$$\boldsymbol{K}_{beam,i} = \begin{pmatrix} \dfrac{A_i}{l_i} & -\dfrac{A_i}{l_i} & 0 & 0 & -\dfrac{B_i}{l_i} & \dfrac{B_i}{l_i} \\ -\dfrac{A_i}{l_i} & \dfrac{A_i}{l_i} & 0 & 0 & \dfrac{B_i}{l_i} & -\dfrac{B_i}{l_i} \\ 0 & 0 & \dfrac{12\Delta_i}{{l_i}^3 A_i} & -\dfrac{12\Delta_i}{{l_i}^3 A_i} & \dfrac{6\Delta_i}{{l_i}^2 A_i} & \dfrac{6\Delta_i}{{l_i}^2 A_i} \\ 0 & 0 & -\dfrac{12\Delta_i}{{l_i}^3 A_i} & \dfrac{12\Delta_i}{{l_i}^3 A_i} & -\dfrac{6\Delta_i}{{l_i}^2 A_i} & -\dfrac{6\Delta_i}{{l_i}^2 A_i} \\ -\dfrac{B_i}{l_i} & \dfrac{B_i}{l_i} & \dfrac{6\Delta_i}{{l_i}^2 A_i} & -\dfrac{6\Delta_i}{{l_i}^2 A_i} & \dfrac{1}{l_i}\left(\dfrac{3\Delta_i}{A_i} + D_i\right) & \dfrac{1}{l_i}\left(\dfrac{3\Delta_i}{A_i} - D_i\right) \\ \dfrac{B_i}{l_i} & -\dfrac{B_i}{l_i} & \dfrac{6\Delta_i}{{l_i}^2 A_i} & -\dfrac{6\Delta_i}{{l_i}^2 A_i} & \dfrac{1}{l_i}\left(\dfrac{3\Delta_i}{A_i} - D_i\right) & \dfrac{1}{l_i}\left(\dfrac{3\Delta_i}{A_i} + D_i\right) \end{pmatrix} \quad i = 1,2 \tag{44}$$

The procedure should be repeated to determine the elementary stiffness matrix of the *bonded-beams* ME associated with of each of four possible adhesive stress solutions given in Eqs (40)–(43). It has been shown in Refs. [83,85] that the same approach is applicable if the Hart-Smith local equilibrium, or a linear adherend shear stress through the thickness according to Tsaï et al. is considered. Only the expressions for some constants need to be changed.

4.3.2. *Variation of simplifying hypotheses*

The initial methodology is well-established. However, a significant effort in terms of mathematical processing and code implementation is

required. In the case where the simplifying hypotheses must be modified (see section 3), it could be attractive to use formulation methodologies avoiding the previous drawbacks associated with the algebraic manipulation of equations. According to this objective, a methodology based on the use of the exponential of matrix is presented in Refs. [85,86]. The governing system of ODEs in Eq. (37) can be written under the matrix shape $\frac{dX}{dx} = \mathscr{A}X$

$$\mathcal{A} = \begin{pmatrix}
0 & 0 & 0 & 0 & 0 & 0 & \frac{D_1}{\Delta_1} & 0 & 0 & 0 & \frac{B_1}{\Delta_1} & 0 \\
0 & 0 & 0 & 0 & 0 & 0 & 0 & \frac{D_2}{\Delta_2} & 0 & 0 & 0 & \frac{B_2}{\Delta_2} \\
0 & 0 & 0 & 0 & 1 & 0 & 0 & 0 & 0 & 0 & 0 & 0 \\
0 & 0 & 0 & 0 & 0 & 1 & 0 & 0 & 0 & 0 & 0 & 0 \\
0 & 0 & 0 & 0 & 0 & 0 & \frac{B_1}{\Delta_1} & 0 & 0 & 0 & \frac{A_1}{\Delta_1} & 0 \\
0 & 0 & 0 & 0 & 0 & 0 & 0 & \frac{B_2}{\Delta_2} & 0 & 0 & 0 & \frac{A_2}{\Delta_2} \\
\frac{G}{e}w & -\frac{G}{e}w & 0 & 0 & \frac{G}{e}wh_1 & \frac{G}{e}wh_2 & 0 & 0 & 0 & 0 & 0 & 0 \\
-\frac{G}{e}w & \frac{G}{e}w & 0 & 0 & -\frac{G}{e}wh_1 & -\frac{G}{e}wh_2 & 0 & 0 & 0 & 0 & 0 & 0 \\
0 & 0 & \frac{E}{e}w & -\frac{E}{e}w & 0 & 0 & 0 & 0 & 0 & 0 & 0 & 0 \\
0 & 0 & -\frac{E}{e}w & \frac{E}{e}w & 0 & 0 & 0 & 0 & 0 & 0 & 0 & 0 \\
\frac{G}{e}wh_1 & -\frac{G}{e}wh_1 & 0 & 0 & \frac{G}{e}wh_1h_1 & \frac{G}{e}wh_1h_1 & 0 & 0 & -1 & 0 & 0 & 0 \\
\frac{G}{e}wh_2 & -\frac{G}{e}wh_2 & 0 & 0 & \frac{G}{e}wh_2h_2 & \frac{G}{e}wh_2h_2 & 0 & 0 & 0 & -1 & 0 & 0
\end{pmatrix} \tag{45}$$

with $X^t=(u_1\, u_2\, v_1\, v_2\, \theta_1\, \theta_2\, N_1\, N_2\, V_1\, V_2\, M_1\, M_2)$ the transposed vector of unknown functions of the overlap abscissa x. The first six rows of $\mathscr{A}$ correspond to the adherend constitutive equations and the last 6 rows to the adherend local equilibrium. The corresponding fundamental matrix of $\mathscr{A}$ is quoted $\Phi_{\mathscr{A}}$ and is defined by its exponential shape $\Phi_{\mathscr{A}}(x) = e^{\mathscr{A}x}$. Two twelve-by-twelve coupling matrices D'_e and L'_e are built from the relevant extractions of the fundamental matrix assessed at both ME extremities in $x=0$ and $x=\Delta$ such as:

$$\begin{cases} D'_e = \begin{pmatrix} [\Phi_{\mathcal{A}}(0)]_{k=1:6,l=1:12} \\ [\Phi_{\mathcal{A}}(\Delta)]_{k=1:6,l=1:12} \end{pmatrix} \\ L'_e = \begin{pmatrix} [\Phi_{\mathcal{A}}(0)]_{k=7:12,l=1:12} \\ [\Phi_{\mathcal{A}}(\Delta)]_{k=7:12,l=1:12} \end{pmatrix} \end{cases} \tag{46}$$

where k stands for the row number and l for the column number. The coupling matrix D_e is then obtained by a simple rearrangement of D_e' lines to be relevant to the sequence of U_e. The coupling matrix L_e is obtained from L_e' by the same rearrangement and by taking the opposite values of matrix components associated with internal loads in $x=0$ (see Eq. (33)). The elementary stiffness matrix of the *bonded-beams* ME is then simply obtained by $K_e = L_e D_e^{-1}$ via a dedicated computer program. It is indicated that the stiffness matrix of beams outside the overlap can be formulated following the same method. As a result, when the matrix $\mathscr{A}$ is written from the chosen simplifying hypotheses, the procedure to generate the corresponding elementary stiffness matrix of the *bonded-beams* ME is simple and straightforward [85,86]. For example, replacement of the local equilibrium of Goland and Reissner by the one of Hart-Smith results in the modification of both moment equations. Only the rows $k = 11$ and $k = 12$ of $\mathscr{A}$ are modified such that:

$$\begin{cases} \mathcal{A}_{11,l} = \left(\frac{G}{e}2b(h_1+h) \quad -\frac{G}{e}2b(h_1+h) \quad 0 \quad 0 \quad \frac{G}{e}2bh_1(h_1+h) \quad \frac{G}{e}2bh_1(h_1+h) \quad 0 \quad 0 \quad -1 \quad 0 \quad 0 \quad 0 \right) \\ \mathcal{A}_{12,l} = \left(\frac{G}{e}2b(h_2+h) \quad -\frac{G}{e}2b(h_2+h) \quad 0 \quad 0 \quad \frac{G}{e}2bh_2(h_2+h) \quad \frac{G}{e}2bh_2(h_2+h) \quad 0 \quad 0 \quad 0 \quad -1 \quad 0 \quad 0 \right) \end{cases} \tag{46a}$$

where h is the half-thickness of the adhesive layer. Another example concerns the replacement of the Euler-Bernoulli beam model by the Timoshenko beam model. In a such case, instead of assuming that the bending angle is equal to the slope of the deflection, the adherend constitutive equation in terms of shear force is used:

$$V_i = H_i\left(\frac{dv_i}{dx} - \theta_i\right) \quad i = 1,2 \tag{47}$$

where H_i is the shear stiffness of adherend i. It is then sufficient to

replace the rows $k = 3$ and $k = 4$ of $\mathscr{A}$ are replaced by:

$$\begin{cases} \mathcal{A}_{3,I} = \begin{pmatrix} 0 & 0 & 0 & 0 & \dfrac{1}{\boldsymbol{H}_1} & 0 & 0 & 0 & \dfrac{1}{\boldsymbol{H}_1} & 0 & 0 & 0 \end{pmatrix} \\ \mathcal{A}_{4,I} = \begin{pmatrix} 0 & 0 & 0 & 0 & \dfrac{1}{\boldsymbol{H}_2} & 0 & 0 & 0 & \dfrac{1}{\boldsymbol{H}_2} & 0 & 0 & 0 \end{pmatrix} \end{cases} \tag{48}$$

To account for the nonlinear bending moment induced by the eccentricity of the load path, a simple approach consists in modifying the length l_i outside of the overlap by Ref. [71]:

$$\boldsymbol{l}' = \frac{1}{\frac{1}{k_M} - 1}\boldsymbol{c} \tag{49}$$

where k_M is the bending moment factor corresponding to the chosen theories (see section 3). Another idea is to implement a ME model corresponding to the theory of Luo and Tong, coupling the adherend normal force and bending moments. The system matrix $\mathscr{A}$ then depends on the applied tensile force f to be transferred and is such as:

$$A = \begin{pmatrix}
0 & 0 & 0 & 0 & 0 & 0 & \frac{1}{2}\left(\frac{D_1}{\Delta_1}+\frac{D_2}{\Delta_2}\right) & \frac{1}{2}\left(\frac{D_1}{\Delta_1}-\frac{D_2}{\Delta_2}\right) & 0 & 0 & \frac{1}{2}\left(\frac{B_1}{\Delta_1}+\frac{B_2}{\Delta_2}\right) & \frac{1}{2}\left(\frac{B_1}{\Delta_1}-\frac{B_2}{\Delta_2}\right) \\
0 & 0 & 0 & 0 & 0 & 0 & \frac{1}{2}\left(\frac{D_1}{\Delta_1}-\frac{D_2}{\Delta_2}\right) & \frac{1}{2}\left(\frac{D_1}{\Delta_1}+\frac{D_2}{\Delta_2}\right) & 0 & 0 & \frac{1}{2}\left(\frac{B_1}{\Delta_1}-\frac{B_2}{\Delta_2}\right) & \frac{1}{2}\left(\frac{B_1}{\Delta_1}+\frac{B_2}{\Delta_2}\right) \\
0 & 0 & 0 & 0 & 1 & 0 & 0 & 0 & 0 & 0 & 0 & 0 \\
0 & 0 & 0 & 0 & 0 & 1 & 0 & 0 & 0 & 0 & 0 & 0 \\
0 & 0 & 0 & 0 & 0 & 0 & \frac{1}{2}\left(\frac{B_1}{\Delta_1}+\frac{B_2}{\Delta_2}\right) & \frac{1}{2}\left(\frac{B_1}{\Delta_1}-\frac{B_2}{\Delta_2}\right) & 0 & 0 & \frac{1}{2}\left(\frac{A_1}{\Delta_1}+\frac{A_2}{\Delta_2}\right) & \frac{1}{2}\left(\frac{A_1}{\Delta_1}-\frac{A_2}{\Delta_2}\right) \\
0 & 0 & 0 & 0 & 0 & 0 & \frac{1}{2}\left(\frac{B_1}{\Delta_1}-\frac{B_2}{\Delta_2}\right) & \frac{1}{2}\left(\frac{B_1}{\Delta_1}+\frac{B_2}{\Delta_2}\right) & 0 & 0 & \frac{1}{2}\left(\frac{A_1}{\Delta_1}-\frac{A_2}{\Delta_2}\right) & \frac{1}{2}\left(\frac{A_1}{\Delta_1}+\frac{A_2}{\Delta_2}\right) \\
0 & 0 & 0 & 0 & 0 & 0 & 0 & 0 & 0 & 0 & 0 & 0 \\
0 & 2\frac{G}{e}w & 0 & 0 & \frac{G}{e}wh_+ & \frac{G}{e}wh_- & 0 & 0 & 0 & 0 & 0 & 0 \\
0 & 0 & 0 & 0 & 0 & 0 & 0 & 0 & 0 & 0 & 0 & 0 \\
0 & 0 & 0 & 2\frac{E}{e}w & 0 & 0 & 0 & 0 & 0 & 0 & 0 & 0 \\
0 & \frac{G}{e}wh_+ & 0 & 0 & \frac{G}{2e}wh_+h_+ + \frac{f}{2} & \frac{G}{2e}wh_+h_- & 0 & 0 & -1 & 0 & 0 & 0 \\
0 & \frac{G}{e}wh_- & 0 & 0 & \frac{G}{2e}wh_+h_- & \frac{G}{2e}wh_-h_- + \frac{f}{2} & 0 & 0 & 0 & -1 & 0 & 0
\end{pmatrix} \tag{50}$$

where $h_+ = h_1+h_2$ et $h\text{-} = h_1\text{-}h_2$. It thus becomes simple to compute K_e when the simplifying hypotheses, which induce a system of linear first order ODEs coupled by the elastic foundation representing for the adhesive layer, vary. However, due to the construction of this formulation methodology, the results are read only at the extremities of the overlap, since the shape of adherend displacement and internal forces, along with adhesive stresses, are not explicitly determined. As a result, the discretization of MEs must be employed if a distribution of results along the overlap is expected. It should be noted that the formulation based on the exponential of matrix was also applied to a multiple-lap joint [89]. It is obvious that the consideration of an unspecified number of adherends bonded by adhesive layers increases the mathematical processing of the governing system of ODEs. By using this formulation methodology, the complexity is confined only to the implementation of the computer program supporting an unspecified number of adherends. Nevertheless, a light dependency on the discretization has been reported. This dependency is not expected and is related to the numerical assessment of the exponential of the matrix system $\mathscr{A}$.

Finally, another formulation methodology based on the use of the Jordan form was published in 2019 [88]. An initial pre-processing of the governing system of first order ODEs is required to obtain a consistent system of higher order ODEs in adherend displacement. Like the exponential method, the governing system is written under a matrix system $\mathscr{A}$ such that $dX/dx = \mathscr{A}X$. The use of the Jordan normal form causes the system to be rewritten as $dZ/dx = JZ$ with $Z = P^{-1}X$. P is an invertible matrix such that $J = P^{-1}\mathscr{A}P$, where J is the Jordan normal form. The Jordan matrix generation relies primarily on the eigenvalues and eigenvectors determination. The number and size of Jordan block are respectively determined by the geometric multiplicity and the nilpotence degree of each eigenvalue. The solution of the initial governing system can be expressed as $X = Pe^{Jx}C$, where C is the integration constants vector. This resolution method offers the ability to express the solution shape of the adherend displacements and internal forces in terms of closed-form but not-ready-to-use equations, such that the results can be obtained at any point without any discretization.

4.3.3. *Exemplification on properties graduation*

The deformability of adherends and adhesive layer leads to peak stresses at the overlap ends (see section 2), such that the load is mainly transferred on a small length compared to the overlap length. A design based on a graduation of mechanical and/or geometrical properties of adherends and/or adhesive could help reduce peak stresses and homogenize the load transfer gradient. For example, the tapering of

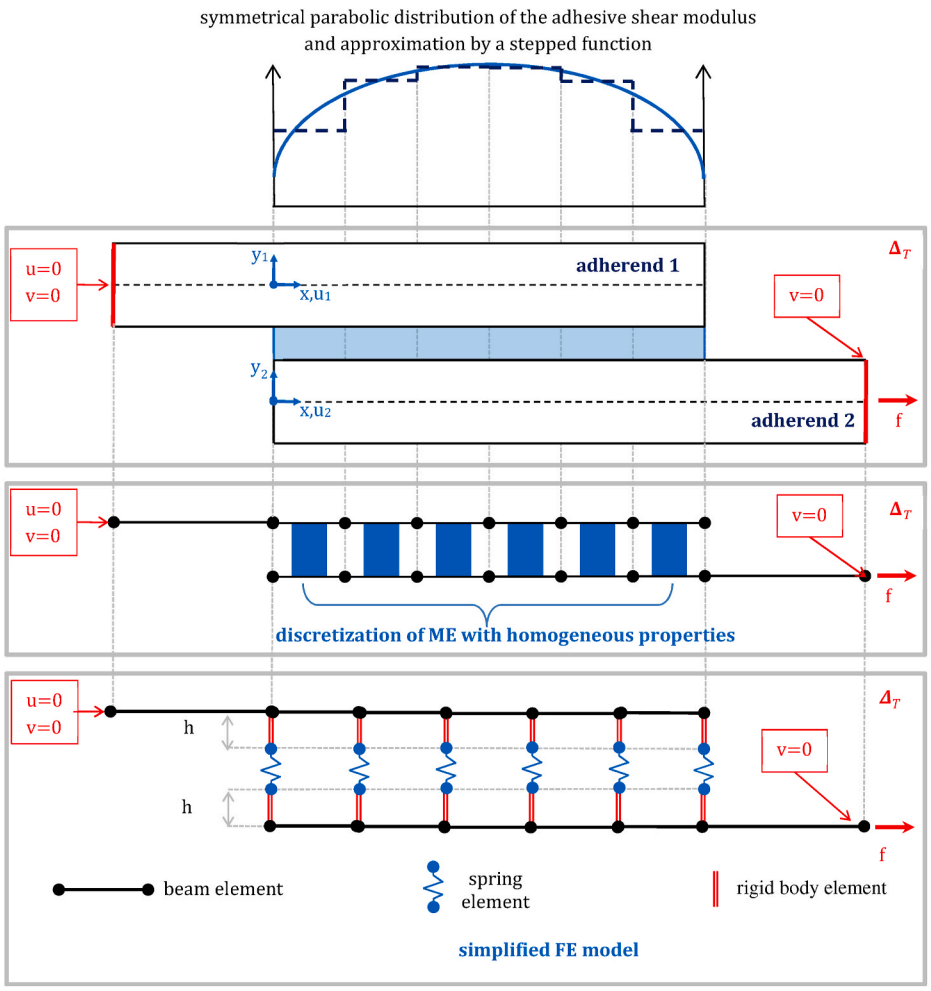

Fig. 12. ME and simplified FE model using homogeneous properties for a single-lap bonded joint involving a symmetrical parabolic distribution of the adhesive shear modulus submitted to combined thermal and mechanical loading.

adherend squared edges allows for a progressive increase in the neutral line lag and bending stiffness, leading to a reduction in adhesive peel stress [112,113]. While the mechanical and/or geometrical properties depend on the overlap abscissa x, however, the governing system of ODEs involves constants depending on x. A solution is to use the ME modelling involving a discretization of ME with homogeneous properties. In such a case, the gradient of properties is approximated by a stepped function. In the context of a 1D-bar ME model, simple

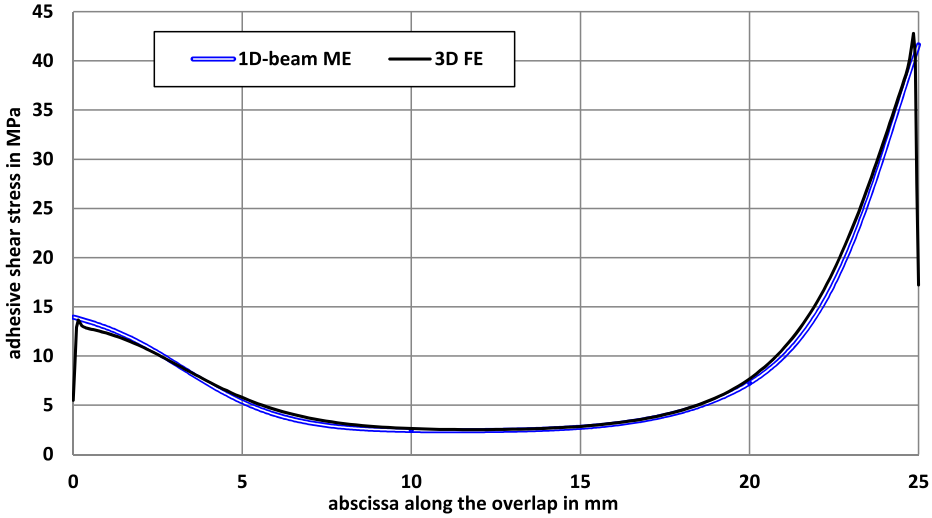

Fig. 13. Adhesive shear stress distribution along the overlap from the 1D-beam ME and FE 3D FE model of an unbalanced single-lap bonded joint (the worst case tested in Ref. [87]).

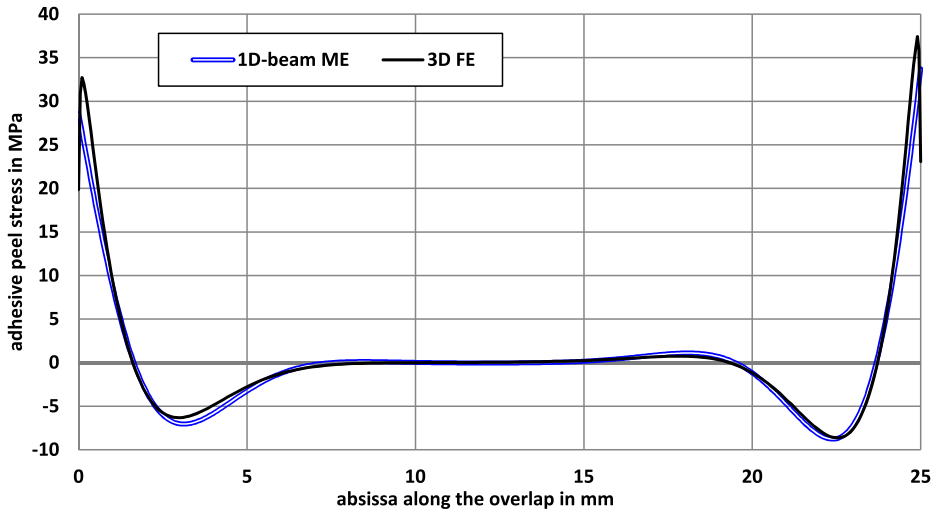

Fig. 14. Adhesive peel stress distribution along the overlap from the 1D-beam ME and FE 3D FE model of an unbalanced single-lap bonded joint (the worst case tested in Ref. [87]).

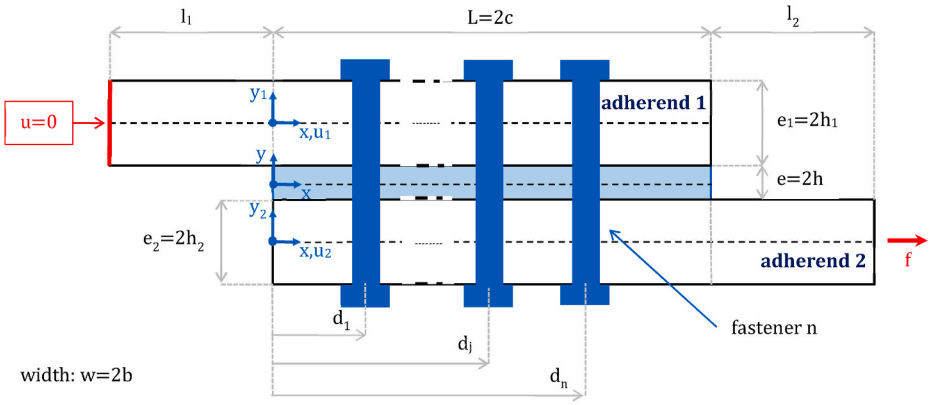

Fig. 15. Scheme and parameterization of single-lap HBB joints with n fastener lines subjected to a tensile force to be transferred.

discretization is sufficient, whereas an additional neutral line lag management step is required for a 1D-beam ME model involving a graduation of the adherend and/or adhesive thickness. By assuming the continuity of adhesive stresses, kinematic relationships can be written at the junction between two successive MEs. For example, the master-slave method allows for the introduction of these kinematics constraints through the application of a reduction matrix. It is indicated that the representation with a beam model of abrupt variations of neutral line

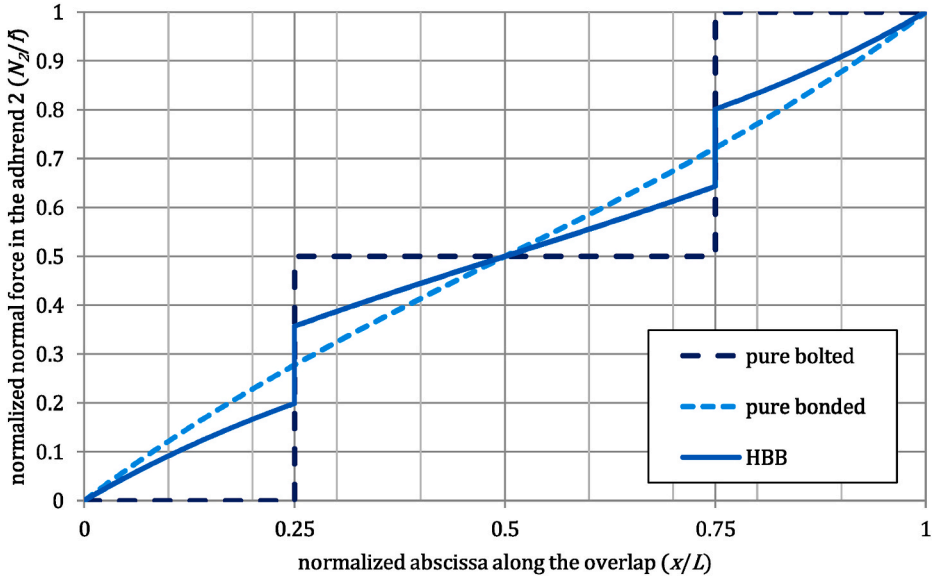

Fig. 16. Load transfer distribution along the overlap for pure bonded and HBB joints.

and/or cross-section areas could lead to numerical results far removed from the observable physical reality.

In this paper, the use of ME modelling is exemplified on the graduation of adhesive properties based on [85,86]. Recently, some simplified stress analyses associated with semi-analytical resolution schemes were published [85,114–116]. The resolution schemes are based on the TEPS, mathematical tool already used by Hart-Smith for the case of stepped or scarfed joints [112]. A 1D-beam ME model based on a discretization of MEs with homogeneous properties for a single-lap bonded joint with a symmetrical parabolic evolution of the adhesive shear modulus is illustrated in Fig. 12. It is assumed that the adhesive Poisson ν ratio remains constant such that the adhesive peel modulus is obtained by multiplying the adhesive shear modulus by $2(1+\nu)$ at each abscissa x. The adherends have the same thickness but are not made from the same materials. It is emphasized that the approach presented is not restricted to this particular graduation shape. The single-lap joint is subjected to combined thermal and mechanical loading. As for the 1D-bar ME analysis, thermal loading is introduced through an elementary equivalent nodal vector $F_{e,th}$ given by Refs. [79,81–85]:

In [86], the ME model results are compared to the results obtained with a simplified FE model. The simplified FE model is designed to be based on the same hypotheses as those of the ME model. The objective of this model is to validate the ME formulation and the associated computer program, since the same hypotheses should give the same results. The formulation based on the exponential of matrix is applied to formulate the elementary stiffness matrix (see section 4.3.2). For a geometrically linear 1D-beam analysis, the ME relevant to the Hart-Smith (Goland and Reissner) model is chosen if the geometrical influence of the adhesive layer is (not) taken into account. The ME relevant to the Luo and Tong model is applied when the FE analysis is geometrically nonlinear. After a convergence study on the number of elements for both the FE and ME models, it is shown that the maximum relative difference with the FE results on maximum adhesive stresses is lower than 1.1% under 1D-beam geometrically linear analysis. It is indicated that these relative differences drop to 0.60% when the adhesive properties are homogeneous. These values lead to the validation of the ME model. It should be noted that the same validation work was performed under 1D-bar analysis in Ref. [86]; a maximum relative difference with the FE results on maximum adhesive shear stresses lower than 0.32% (0.01%) is obtained when the adhesive properties are graduated (homogeneous). Moreover, it was shown that an overlap length, minimizing the maximum adhesive shear stress, exists. Besides, when geometrically nonlinear 1D-beam analyses are run, the ME model makes use of the ME formulated following the Luo and Tong model involving an approximation of large displacements (see section 4.3.2). It is interesting to note that the ME model based on the Luo and Tong approach leads to small relative differences without any iterative procedure. Moreover, an evaluation of the ME model results compared to refined 3D models is presented in Ref. [86]. Brick elements (cohesive elements) are used for the adhesive layer in the FE model if it is decided (not) to take into account the geometrical presence of the adhesive thickness. The maximum relative differences fall between 0.82% and 7.88% for the maximum adhesive shear stress and between 1.36% and 17.5% for the adhesive peeling stresses, depending on the tested cases.

$$\boldsymbol{F}_{e,th}{}^{t} = \left(-\boldsymbol{N}_1^{\Delta_T} \quad -\boldsymbol{N}_2^{\Delta_T} \quad \boldsymbol{N}_1^{\Delta_T} \quad \boldsymbol{N}_2^{\Delta_T} \quad 0 \quad 0 \quad 0 \quad 0 \quad \boldsymbol{M}_1^{\Delta_T} \quad \boldsymbol{M}_2^{\Delta_T} \quad -\boldsymbol{M}_1^{\Delta_T} \quad -\boldsymbol{M}_2^{\Delta_T} \right) \tag{51}$$

where $N_i^{\Delta_T}$ and $M_i^{\Delta_T}$ are respectively the normal force and the bending moment in the adherend i due to a uniform target temperature variation Δ_T. Their expressions are as follows:

$$\begin{cases} N_i^{\Delta_T} = w \sum_{p_i=1}^{n_i} Q_i^{p_i} \alpha_i^{p_i} \left(h_{p_i} - h_{p_i-1} \right) \Delta_T \\ \\ M_i^{\Delta_T} = \dfrac{w}{2} \sum_{p_i=1}^{n_i} Q_i^{p_i} \widehat{\alpha}_i^{p_i} \left(h_{p_i}{}^2 - h_{p_i-1}{}^2 \right) \Delta_T \end{cases} \qquad i = 1,2 \tag{52}$$

where, for a laminated adherend with p_i plys, each ply has a reduced modulus along the x-axis $Q_i^{p_i}$, at thickness $h_{p_i} - h_{p_i-1}$ and $\alpha_i^{p_i}$ as thermal expansion coefficients. If the laminated adherend has a mirror symmetry, then $B_i = 0$ and $M_i^{\Delta_T} = 0$.

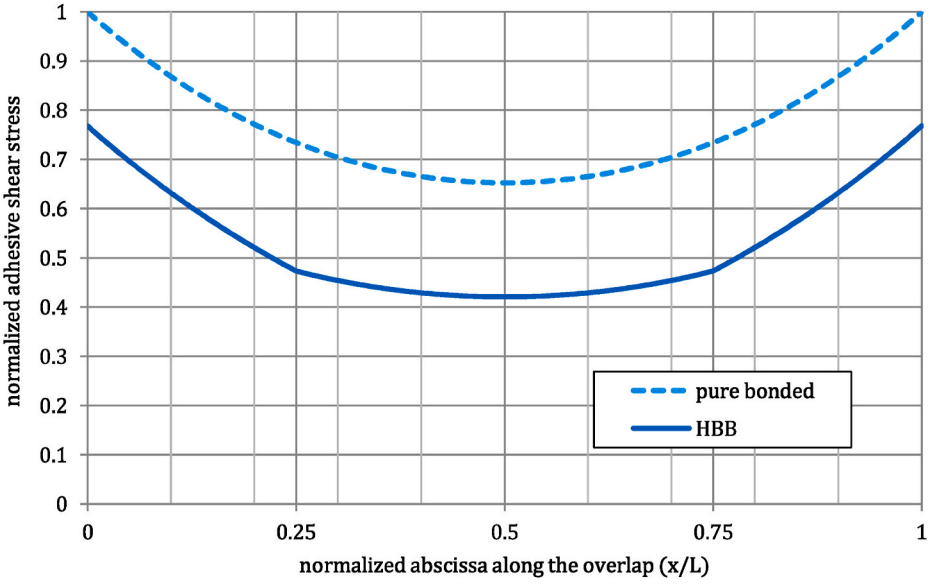

Fig. 17. Adhesive shear stress distribution along the overlap for pure bonded and HBB joints.

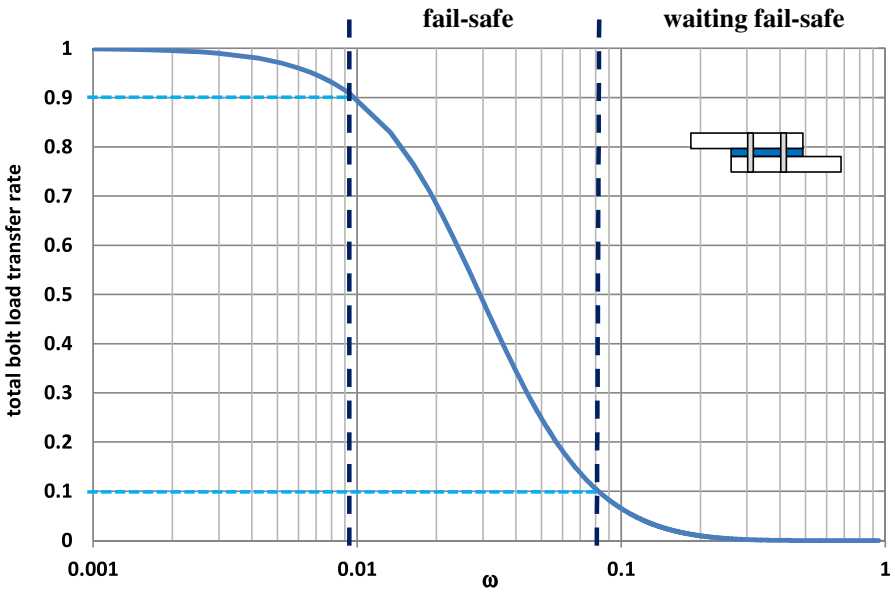

Fig. 18. Total bolt load transfer in a two-fastener lines HBB joint made of similar adherends as a function of ω. The dashed lines clearly highlight the three different working regions, based on the authors' specific choice of bolt load transferred.

No significant influence of the graduation of adhesive properties on the relative differences was shown. The maximum relative difference is obtained when the adhesive physical thickness is subjected to a geometrically nonlinear analysis. To illustrate the comparisons performed in Ref. [87], the distribution of the adhesive shear and peel stress along the overlap coming from the 1D-beam ME and 3D FE analyses are provided in Fig. 13 and Fig. 14. The worst case in terms of relative difference in peel stress among the tested cases in Ref. [87] is chosen. This corresponds to an unbalanced single-lap joint under pure mechanical loading and involving a symmetrical parabolic graduation of the adhesive peel and shear modulus. The adhesive layer is modelled in the 3D FE model with brick elements and the adhesive stresses are measured at the middle of the adhesive layer. The FE analysis is geometrically nonlinear. To approximate the tested configuration, the 1D-beam ME is based on the Luo and Tong local equilibrium, in which the adhesive thickness is taken into account in the bending moment equation following Hart-Smith.

Finally, in 2020, a formulation methodology based on TEPS was presented [90,91]. The unknown adherend displacements are expanded in power series. An initial solution is to consider the governing system of first order ODEs as for the formulation using the exponential of matrix (see section 4.3.2). In this case, the adherend internal loads are then expanded in power series too. A second solution requires the pre-processing of ODEs to determine a system of higher order ODEs in the adherend displacement only, as for the formulation based on the Jordan form (see section 4.3.2). In this case, the expansions in power series of adherend internal loads are deduced from those of displacements using the constitutive equations. In both cases, the set of ODEs lead to recursive equations whose unknowns are the series terms. The adherend nodal displacements and internal loads can then be written as functions of the unknown series terms. After truncating the series to an order N, coupling matrices depending on N $D_e^{-1}(N)$ and $L_e(N)$ can be written, leading to the elementary stiffness matrix $K_e(N)$ as a function of the order of truncation. A convergence study of the truncation order is then required to determine a suitable value for N. This methodology allows for the formulation of the elementary stiffness matrix of *bonded-bars* and *bonded-beams* ME including the graduation of the adhesive properties, which is expanded in power series. When the adhesive properties are expanded in power series, series products appear and are handled thanks to the Cauchy product, then allowing the treatment of

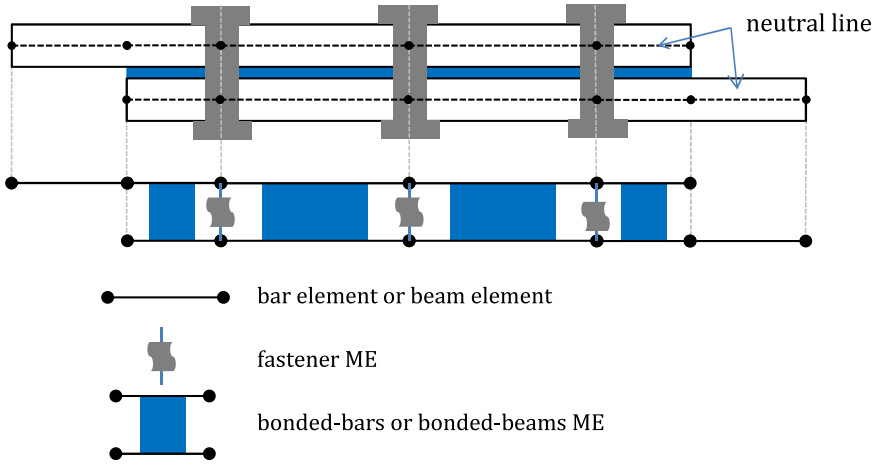

Fig. 19. ME model for a single-lap HBB joint with three lines of fasteners.

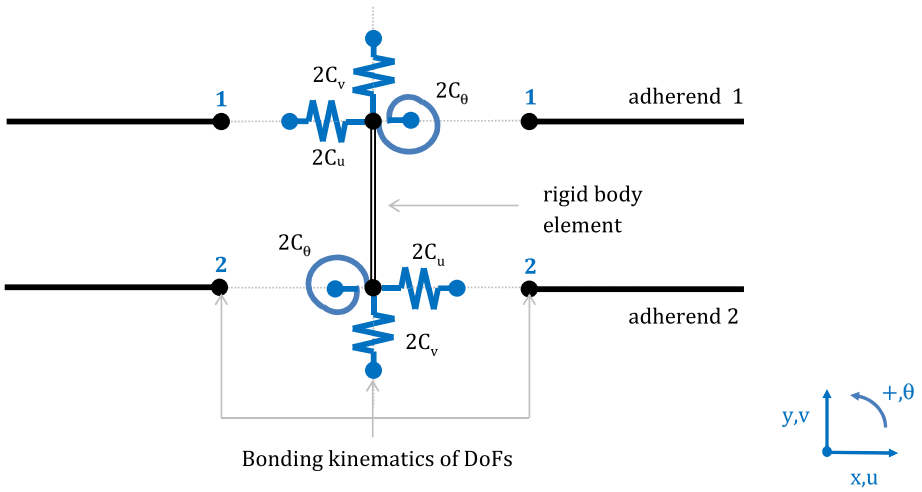

Fig. 20. Fastener ME under 1D-beam analysis.

the nonlinearity in the ODEs induced by the graduation of adhesive properties. In other words, when including a graduation of adhesive properties, the ME model with TEPS formulation-based ME requires only one ME for the entire overlap. In 2021, this formulation was extended to multiple-lap joints involving graduated mechanical and/or geometrical parameters under 1D-beam and cylindrical bending plate following Mortensen and Thomsen [117]. In particular, for the case of the 1D-beam multiple-lap joint, the formulation based on TEPS is no longer dependent on discretization, contrary to the formulation based on the exponential of matrix.

5. Application to hybrid (bolted/bonded) joints

5.1. Shear-lag approach

A single-lap HBB joint with n fastener lines subjected to a tensile force to be transferred is under consideration (see Fig. 15). For n fasteners, there are n+1 bonded bays located between $d_{j\text{-}1}$ and d_j, where d_j (j = 1..n) is the abscissa at which the jth fastener is located, $d_0 = 0$ and $d_{n+1} = L$. In addition to the simplifying hypotheses of the shear-lag model for bonded joints following Arnovljevic or Volkersen (see section 2.1.1), it is assumed that the fasteners are linear elastic and modelled by a shear spring connecting both adherend neutral lines. The previous hypotheses for the fasteners correspond to those used within the models developed at NACA after the Second World War [6–8] (see section 1). A semi-analytical resolution scheme based on the integration of the governing system ODEs was presented in Refs. [74,76,78,80].

The method consists in analysing each bonded bay following the model by Arnovljevic or Volkesersen. The normal force on the jth bonded sandwich of adherend 2, quoted $N_{2,j}$ is then expressed as:

$$N_{2,j} = c_{2j-1}e^{-\eta x} + c_{2j}e^{\eta x} + \frac{\xi}{1+\xi}f \; j = 1..n+1 \tag{53}$$

where $c_{2j\text{-}1}$ and c_{2j} ($j = 1..n$+1) are integration constants. As a result, a total of 2*(n+1) integration constants must be identified. By assuming (i) the continuity of the adhesive stresses at fastener lines, (ii) the load transferred by each fastener, and (iii) the values of the normal force in adherend 2 in $x = 0$ and $x = L$, $n + n$+2 = 2*(n+1) equations are

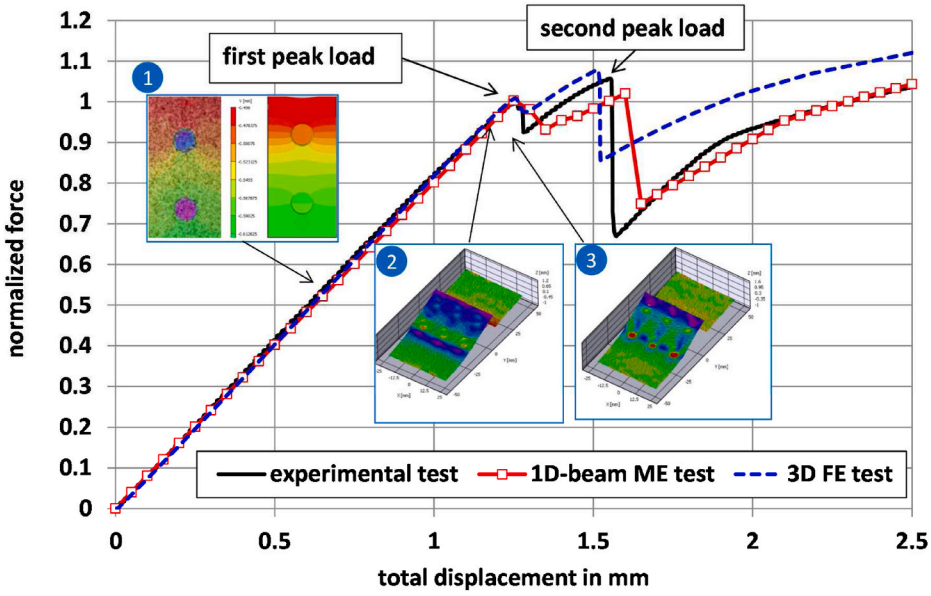

Fig. 21. Normalized load as a function of total specimen displacement measured experimentally and simulated by a 1D-beam ME and 3D FE model. The picture denoted 1 represents the longitudinal strain along the load direction measured by stereo-correlation and simulated by a 3D FE model. The pictures denoted 2 and 3 represent the deflection measured by stereo-correlation before and after the first load peak.

obtained. The following linear system is then deduced:

$$\begin{cases} c_1 + c_2 = -\dfrac{\xi}{1+\xi} f \\ e^{-\eta d_j} c_{2j-1} - e^{\eta d_j} c_{2j} - e^{-\eta d_j} c_{2j+1} + e^{\eta d_j} c_{2j+1} = 0 \quad j = 1 \ldots n \\ (1-\varphi_j) e^{-\eta d_j} c_{2j-1} + (1+\varphi_j) e^{\eta d_j} c_{2j} - e^{-\eta d_j} c_{2j+1} - e^{\eta d_j} c_{2j+1} = 0 \quad j = 1 \ldots n \\ c_{2n+1} + c_{2n+2} = \dfrac{1}{1+\xi} f \end{cases} \tag{54}$$

where:

$$\varphi_j = C_j \frac{e}{G} \frac{\eta}{w} \quad j = 1 \ldots n \tag{55}$$

and C_j is the fastener stiffness of the jth fastener. Numerous fastener stiffness formulae exist, such as for example [7,118–120]. The bolt load transfer rate of the jth fastener is denoted τ_j and is given by:

$$\tau_j f = \varphi_j \left(- c_{2j-1} e^{-\eta d_j} + c_{2j} e^{\eta d_j} \right) \quad j = 1 \ldots n \tag{56}$$

Needless to say, a linear variation of the adherend shear stress through the thickness following Tsaï et al. [18] can be introduced adapting the adhesive shear modulus following section 2.1.4.

For illustrative purposes, the normalized load transfer distribution along the overlap for a pure bonded, pure bolted and HBB joint made of similar adherends and having the same overlap length is provided in Fig. 16. For pure bonded and HBB joints, the distributions of adhesive shear stress divided by the maximum adhesive shear stress of the pure bonded configuration is provided in Fig. 17 along the overlap length. Two lines of fasteners are considered for the bolted and HBB joints. The load transfer mode is then both continuous along the bonded bay and discrete at the fastener lines. The presence of the adhesive layer allows the load transferred by the fasteners to be reduced. Consequently, the bearing stress and fastener shear stress are also reduced. The net-section stress at the fastener hole is reduced due to the load transferred by the adhesive between the overlap end and the fastener. As a result, while the adhesive layer sustains the load without cracking, the static strength of the HBB joint is expected to be higher than the one of the pure bolted joint. For the HBB joint, the adhesive shear stress distribution along the overlap is continuous along the overlap, with singularities at the fastener locations, due to the discrete load transfer. The area under the adhesive shear stress curve is equal to the tensile flow transferred by the adhesive: it means $(1\text{-}\tau_1\text{-}\tau_2)\varphi$. The maximum adhesive shear stress in the HBB joint is then lower than in the pure bonded joint, while remaining located at both overlap ends.

The linear system in Eq. (54) can be solved analytically leading to closed-form and ready-to-use equations for bolt load transfer rates, and maximum adhesive stresses under specific conditions. For example, for the case of an HBB joint with two similar fasteners (having the same stiffness C_1=C_2=C_F), made of two similar adherends and such $d_1 = L\text{-}d_2$:

$$\tau_1 f = \tau_2 f = \frac{1}{2} \frac{\bar{r} + \bar{q}}{\bar{r} e^{\eta d_1} - \bar{q} e^{-\eta d_1}} \frac{\eta C_F}{G} \frac{e}{w} f \tag{57}$$

where:

$$\bar{r} = -1 + \cosh \eta (L - 2d_1) - (1+\varphi_1) \sinh \eta (L - 2d_1) \tag{58}$$

$$\bar{q} = 1 - \cosh \eta (L - 2d_1) + (1-\varphi_1) \sinh \eta (L - 2d_1) \tag{59}$$

The closed-form solution for the maximum shear stress is:

$$T_{max} = \frac{1}{2} \frac{\bar{r} e^{\eta d_1} + \bar{q} e^{-\eta d_1}}{\bar{r} e^{\eta d_1} - \bar{q} e^{-\eta d_1}} \eta \varphi = \omega \frac{\bar{r} e^{\omega \frac{d_1}{c}} + \bar{q} e^{-\omega \frac{d_1}{c}}}{\bar{r} e^{\omega \frac{d_1}{c}} - \bar{q} e^{-\omega \frac{d_1}{c}}} T_{av} \tag{60}$$

Thanks to the model presented, it is possible to quickly perform influence studies of the design parameter on the load transfer shared between the fasteners and the adhesive layer. For example, the influence of the parameter ω on the total load transferred by the fasteners can be drawn (Fig. 18). It is reminded that ω represents the ratio between the adhesive shear stiffness with the membrane stiffness of both adherends (see section 2.1.2, Eq. (9)). Without limiting the generalities of the observations made, the curve given in Fig. 18 is related to an HBB joint with fastener lines, for which the mechanical and material properties are fixed, with the exception of the adhesive shear modulus, which varies allowing for the variation of ω. When the adhesive shear stiffness is significantly lower before the adherend membrane stiffness (very low ω), the fasteners mainly transfer the load, such that the HBB joint behaves like a pure bolted joint. A bolted-sealed joint may be an example. When the adhesive shear stiffness cannot be neglected due to the membrane stiffness of the adherend (ω close to 1), the load is transferred by the adhesive layer, such that the HBB joint behaves like a pure bonded joint. In other words, the fasteners could transfer the load only if the adhesive layer becomes sufficiently damaged. This design philosophy can then be qualified as *waiting fail-safe*. For intermediate values of ω, the load is shared between the fasteners and the adhesive. The adhesive layer can then be regarded as an additional load path relevant to a *fail-safe* design philosophy. Numerous publications, involving adherends made of metallic or composite laminate materials, along with various manufacturing processes [74,121–142] (without claiming to be exhaustive), have shown that the HBB design solution compared to pure bolted or pure bonded design solutions, can significantly increase the static strength and fatigue strength for a judicious choice of adhesive.

5.2. Macro-element modelling

ME modelling was initially created to simplify the stress analysis of HBB joints. The idea is to discretize the overlap with *bonded-bars* or *bonded-beams* MEs and fastener MEs to respectively represent the bonded bays and the fasteners (see Fig. 19). The elementary stiffness matrices of fastener MEs under 1D-bar and 1D-beam analyses have been formulated.

In the case of a 1D-bar analysis, the fastener is modelled as a shear spring following the NACA models [6–8]. The elementary stiffness matrix $K_{e,fast}$ is then simply defined by:

$$K_{e\,fast} = C_F \begin{pmatrix} 1 & -1 \\ -1 & 1 \end{pmatrix} \tag{61}$$

In the case of a 1D-beam analysis, the fastener is modelled by a rigid body element associated with two identical triplets of springs, whose stiffness's are ($2C_u$; $2C_v$; $2C\theta$), as illustrated in Fig. 20 [74,76,78]. A rigid body element ensures the displacement continuity between the adherends. With k = 1,2 by denoting $F_u(k)$ and $F_v(k)$ the nodal forces according to the x-axis and y-axis respectively, $F\theta(k)$ the moment around the z-axis, $u(k)$ and $v(k)$ the nodal displacement according to the x-axis and y-axis respectively and $\theta(k)$ the nodal rotation around the z-axis, the elementary stiffness matrix of the fastener ME linking the elementary nodal and displacement vectors [79] is:

$$\begin{pmatrix} F_u(1) \\ F_u(2) \\ F_v(1) \\ F_v(2) \\ F_\theta(1) \\ F_\theta(2) \end{pmatrix} = K_{e\,fast} \begin{pmatrix} u(1) \\ u(2) \\ v(1) \\ v(2) \\ \theta(1) \\ \theta(2) \end{pmatrix} \tag{62}$$

where:

$$\boldsymbol{K}_{e\_fast}=\begin{pmatrix} \frac{2C_uC_\theta}{\overline{C}} & -\frac{2C_uC_\theta}{\overline{C}} & 0 & 0 & -h_+\frac{2C_uC_\theta}{\overline{C}} & -h_+\frac{2C_uC_\theta}{\overline{C}} \\ -\frac{2C_uC_\theta}{\overline{C}} & \frac{2C_uC_\theta}{\overline{C}} & 0 & 0 & h_+\frac{2C_uC_\theta}{\overline{C}} & h_+\frac{2C_uC_\theta}{\overline{C}} \\ 0 & 0 & C_v & -C_v & 0 & 0 \\ 0 & 0 & -C_v & C_v & 0 & 0 \\ -h_+\frac{2C_uC_\theta}{\overline{C}} & h_+\frac{2C_uC_\theta}{\overline{C}} & 0 & 0 & \frac{2C_\theta^2+h_+^2C_uC_\theta}{\overline{C}} & -\frac{2C_\theta^2}{\overline{C}} \\ -h_+\frac{2C_uC_\theta}{\overline{C}} & h_+\frac{2C_uC_\theta}{\overline{C}} & 0 & 0 & -\frac{2C_\theta^2}{\overline{C}} & \frac{2C_\theta^2+h_+^2C_uC_\theta}{\overline{C}} \end{pmatrix} \tag{63}$$

$$\overline{C}=2C_\theta+\frac{1}{2}h_+^2C_u \tag{64}$$

The parameter $h_+ = h_1+h_2$ then represents, for the neutral line lag.

5.3. Experimental and numerical quasi-static test

In Paroissien et al. [79], both experimental and numerical 1D-beam ME and 3D FE quasi-static tests up to failure on the single-lap HBB joint subjected to a tensile force with two lines and three rows of fasteners are presented. Even though the experimental and numerical test procedures and results are detailed in Ref. [79], a summary is given in this section.

The adherends are similar and made of 2024-T351 aluminium alloys. A room temperature curing two-component methacrylate adhesive from LORD Corporation is used. The adherends are drilled before applying the adhesive. After cleaning and degreasing the surface of the adherends to be bonded, the adhesive is applied to one adherend surface. The mechanical fastening system consists of a titanium TA6V countersunk head screw with a shank diameter Φ_F = 5.56 mm (prEN6114-V-3A-4) and steels nuts (ASNA2531-3A). A net fit installation of fasteners is performed (10 μm ± 10 μm). The fasteners are torqued at 1 N m on wet adhesive. As a result, the adhesive thickness is not constant along the overlap.

A 250 kN Instron hydraulic tensile machine is used. The loading is applied through controlled displacement at a rate of 1 mm/min. The specimen is clamped on spacers with hydraulic grips. A full-field displacement measurement through digital image correlation is installed in front the specimen. The system is focused on the overlap area and countersunk head side. A calibrated random pattern with a convenient contrast is painted before the test.

The retrieved displacement as a function of the total displacement of the specimen measured by the tensile machine is given in Fig. 21. A linear behaviour is shown up to an initial peak load. The value of this peak load is used as a reference force to normalize the force in Fig. 21. The load drop is approximately 8% before load recovery up to a second peak load approximately 6% higher than the first load peak. The next load drop is approximately 32% lower than the first load peak. Finally, a nonlinear load recovery is observed up to force at failure approximately 4% higher than the first load peak. The failure is due to the failure of screws in the filets. The pictures denoted 2 and 3 in Fig. 21 provided the deflection measured by stereo-correlation before and after the first load peak. They clearly indicate that the first load drop is due to the failure of the adhesive layer between both edge distances. Similarly, the second peak load corresponds to the failure of the adhesive over the entire overlap, such that the load is only transferred by the fasteners during the second load recovery phase.

A 1D-beam ME model and a 3D FE model have been developed in order to simulate the experimental test. In the context of ME modelling, a Newton-Raphson iterative algorithm based on the secant matrix was implemented by Lélias et al. [84,85]. As the adhesive layer is modelled by an elastic foundation, when damage evolution laws are used for the adhesive constitutive law, the adhesive layer in the ME modelling is equivalent to cohesive zone modelling, which is commonly used to simulate the progressive debonding of interfaces. This algorithm was employed and validated for the simulation of the delamination of composite laminates [89] as well as for of the debonding of fracture mechanics specimens and single-lap joints [143]. In this paper, the traction separation laws are assumed to be bilinear on each of both pure modes, with linear energetic interaction laws for both initiation and propagation. The definition of both pure mode traction separation laws is chosen to ensure the correct dissipation of energy [144], such that five parameters must be defined. These five parameters are not experimentally identified, but numerically calibrated to best fit the experimental results measured on the experimental test of the HBB joint. Consequently, they cannot be considered as intrinsic material parameters. The fastener stiffness is set to $C_v = \frac{E_f \pi \varphi_f^2}{4h_+}$ where E_f is the screw Young's modulus. According to Ref. [74] and following [120], the fastener stiffness $C\theta$ is deduced from C_u by $C_\theta = \frac{3}{8}(1+\nu_f)\varphi_F^2 C_u$ where ν_f the fastener Poisson ratio. To simulate the nonlinear behaviour during the second load recovery, a bilinear law with positive hardening is used for the fastener law along the x-direction. In other words, the relationship between the bolt load along the x-axis and the displacement is linear with a slope $C_{u1}>0$ up to a displacement $\delta_{u1}>0$ followed by a second linear evolution with a slope C_{u2} such as $0<C_{u2}<C_{u1}$. As for the adhesive law parameters, the three parameters C_{u1}, C_{u2} and δ_{u1} are adjusted to best fit the experimental test results. In the context of the 3D FE model, the adherends, screws and nuts are meshed with linear eight-mode brick elements under full integration. The adherends and screws are simulated by elastic perfectly plastic laws using the Von Misès yield criterion. The nuts are assumed to be linear elastic. The adhesive layer is modelled with interface elements; the adhesive traction separation laws in both pure modes as well as the initiation interaction laws are the same as for the ME model. The Benzeggagh-Kenane criterion is used for the propagation interaction law. Comparison between the 1D-beam ME and 3D FE numerical test results and the experimental test results shows a good agreement of the force displacement curve (Fig. 21). The picture denoted 1 in Fig. 21 represents the longitudinal strain measured by stereo-correlation and computed by the 3D FE model: a good agreement is shown. Moreover, the progressive failure scenario observed during the experimental test is reproduced by both numerical tests.

We can conclude that the 1D-beam ME model is a relevant approach to simulating the mechanical behaviour of HBB joints at low computational time. Other more or less complicated semi-analytical approaches can be found in the literature [127,145].

6. Conclusion

At first sight, the mechanical behaviour of two slender structural parts bonded by an adhesive layer and subjected to tensile load could appear simple to grasp, due to the potential simplifications on the stress and strain tensors that could be made. For over a century however, numerous works have been published. It has been shown that the mathematical treatment of ordinary differential equations deduced from the simplifying hypotheses is complicated. Thus, the scope of closed-form and ready-to-use solutions is restricted. The use of semi-analytical resolution schemes appears necessary to extend this scope, even for one-dimensional cases. The choice of simplifying hypotheses also appears to be relevant. The development of semi-analytical resolution schemes, such as the ME approach, allowing the enrichment of models to be ever closer to the physical reality, could reduce the computational time, while providing access to an accurate description of the mechanical behaviour. Additionally, it is highlighted that ME modelling can be used to address the preliminary design of various in-plane loaded structural parts made of bars, beams, fasteners and (multi-)layered bars and beams. The loads can be applied in the form of force or displacement, while combined with a uniform target temperature variation. Moreover, nonlinear homogeneous and graduated

material behaviours can be included in the analysis, in particular allowing for the simulation of progressive joint failure.

In the context of a design process, stress analyses only provide mechanical fields susceptible to be used as input data of strength criteria. These strength criteria could be obtained theoretically and/or experimentally while involving safety factors calibrated with the real in-service life. Moreover, they must be determined in view of the selected design philosophy and by considering the adhesive bonding system defined by the adhesive, the adherends and the manufacturing process. The results of stress analyses are obviously dependent on the material properties of the adhesive employed such as a confined layer [146,147], considering that these material properties can influence the resolution scheme to be used.

Declaration of competing interest

The authors declare that they have no known competing financial interests or personal relationships that could have appeared to influence the work reported in this paper.

Acknowledgement

This work has not received any specific grant. The authors would like to thank Professor Michel Salaün for his valuable help in the preparation of the revised manuscript.

References

[1] A. Higgins, Adhesive bonding of aircraft structures, Int. J. Adhesion Adhes. 20 (2000) 367–376, https://doi.org/10.1016/S0143-7496(00)00006-3.
[2] N. de Bruyne, The strength of glued joints, Aircraft Eng. Aero. Technol. 16 (4) (1944) 115–118, https://doi.org/10.1108/eb031117.
[3] L.R. Demarkles, Investigation of the Use of a Rubber Analog in the Study of Stress Distribution in Riveted and Cemented Joints, NACA TN-3413, 1955. Washington (DC), https://ntrs.nasa.gov/api/citations/19930084165/downloads/19930084165.pdf.
[4] I. Arnovljevic, Das verteilungsgesetz der Tiefspannungen in axial beanspruchten verbundstaben, Z.F. Archund-Ing-Wesen 55 (1909) 415–418.
[5] O. Volkersen, Die Nietkraftverteilung in Zugbeanspruchten Nietverbindungen mit konstanten Laschenquerschnitten, Luftfahrforschung 15 (24) (1938) 41–47.
[6] R.D. Ross, An Electrical Computer for the Solution of Shear-Lag and Bolted Joints Problems, NACA, TN-1281, 1946. Langley Field (VA), https://ntrs.nasa.gov/api/citations/19930081897/downloads/19930081897.pdf.
[7] M.B. Tate, S.J. Rosenfeld, Preliminary Investigation of the Loads Carried by Individual Bolts in Bolted Joints, NACA TN-1051, 1946. Langley Field (VA), https://ntrs.nasa.gov/api/citations/19930081668/downloads/19930081668.pdf.
[8] S.J. Rosenfeld, Analytical and Experimental Investigation of Bolted Joints. NACA TN-1458, 1947. Washington (DC), https://ntrs.nasa.gov/api/citations/19930082094/downloads/19930082094.pdf.
[9] J.F.P. Owens, P. Lee-Sullivan, Stiffness behavior due to fracture in adhesively bonded composite-to-aluminum joints. I. Theoretical model, Int. J. Adhesion Adhes. 20 (2000) 39–45, https://doi.org/10.1016/S0143-7496(99)00013-5.
[10] R.D. Adams, N.A. Peppiatt, Stress analysis of adhesive-bonded lap joints, J. Strain Anal. Eng. Des. 8 (2) (1973) 185–196, https://doi.org/10.1243/03093247V093185.
[11] R.D. Adams, N.A. Peppiatt, Effect of Poisson's ratio in adherends on stresses of an idealized lap joint, J. Strain Anal. Eng. Des. 9 (3) (1974) 134–139, https://doi.org/10.1243/03093247V082134.
[12] X. Xiao, P.H. Foss, J.A. Schroeder, Stiffness prediction of the double lap shear joint. Part1: analytical solution, Int. J. Adhesion Adhes. 24 (2004) 229–237, https://doi.org/10.1016/j.ijadhadh.2003.10.003.
[13] W. Li, E. Ghafoori, Y. Lu, S. Li, M. Motavalli, Analytical solution for stiffness prediction of bonded CFRP-to-steel double strap joints, Eng. Struct. 177 (2018) 190–197, https://doi.org/10.1016/j.engstruct.2018.09.024.
[14] Adhesives — Determination of Shear Behaviour of Structural Adhesives — Part 2: Tensile Test Method Using Thick Adherends, ISO 11003-2:2019.
[15] O. Volkersen, Recherche sur la théorie des assemblages collés, Constr. Met. (CTICM) 4 (1965) 3–13.
[16] L.J. Hart-Smith, Adhesive-bonded Double-Lap Joints, NASA Contractor Report, CR-112235, 1973. Douglas Aircraft Company Long Beach (CA), https://ntrs.nasa.gov/api/citations/19740005082/downloads/19740005082.pdf.
[17] W.T. Chen, C.W. Nelson, Thermal stress in bonded joints, IBM J. Res. Dev. 23 (2) (1979) 179–188, https://doi.org/10.1147/rd.232.0179.
[18] M.Y. Tsaï, D.W. Oplinger, J. Morton, Improved theoretical solutions for adhesive lap joints, Int. J. Solid Struct. 35 (1998) 1163–1185, https://doi.org/10.1016/S0020-7683(97)00097-8.
[19] E. Suhir, Stresses in bi-metal thermostats, J. Appl. Mech. 53 (1986) 657–660, https://doi.org/10.1115/1.3171827.
[20] E. Suhir, An approximate analysis of multilayered elastic thin films, Mater. Res. Soc. Proc. 72 "Electronic Packaging Mater. Sci. II" (1986) 133–136, https://doi.org/10.1115/1.3173620.
[21] E. Suhir, Stresses in adhesively bonded bi-material assemblies used in electronic packaging, J. Appl. Mech. 51 (1988) 143–148, https://doi.org/10.1115/1.3173620.
[22] S.P. Timoshenko, Analysis of bi-metal thermostats, J. Opt. Soc. Am. 11 (3) (1925) 233–255, https://doi.org/10.1364/JOSA.11.000233.
[23] Y. Gilibert, A. Rigolot, Analyse asymptotique des assemblages collés à double recouvrement, sollicités au cisaillement, en traction, J. Mec. Theor. Appl. 3 (3) (1979) 341–372.
[24] Y. Gilibert, A. Rigolot, Théorie élastique de l'assemblage collé à double recouvrement: utilisation de la méthode des développements asymptotiques raccordés au voisinage des extrémités, Mater. Struct. 5 (18) (1985) 363–387, https://doi.org/10.1007/bf02472407.
[25] L.J. Hart-Smith, Adhesive-bonded Single-Lap Joints, NASA Contractor Report, CR-112236, 1973. Douglas Aircraft Company Long Beach (CA), https://ntrs.nasa.gov/api/citations/19740005083/downloads/19740005083.pdf.
[26] M. Goland, E. Reissner, The stresses in cemented joints, J. Appl. Mech. (1944) 11 A17–A27.
[27] J. Jumel, M.K. Budzik, M.E. Shanahan, Beam on elastic foundation with anti-clastic curvature: application to analysis of mode I fracture tests, Eng. Fract. Mech. 78 (18) (2011) 3253–3269, https://doi.org/10.1016/j.engfracmech.2011.09.014.
[28] M. Cabello, J. Zurbitu, J. Renart, A. Turon, F. Martinez, A general analytical model based on elastic foundation beam theory for adhesively bonded DCB joints either with flexible or rigid adhesives, Int. J. Solid Struct. 94–95 (2016) 21–34, https://doi.org/10.1016/j.ijsolstr.2016.05.011.
[29] E. Suhir, Interfacial stresses in bi-metal thermostats, J. Appl. Mech. 56 (1989) 595–600, https://doi.org/10.1115/1.3176133.
[30] J. Zhang, In-process Stress Analysis of Flip Chip Assembly and Reliability Assessment during Environmental and Power Cycling, PhD Dissertation, 2003. Georgia Institute of Technology Atlanta (GA), http://hdl.handle.net/1853/5442.
[31] J.W. van Ingen, A. Vlot, Stress Analysis of Adhesively Bonded Single-Lap joints., TU Delft, Report LR-740, 1993. Delft (NL), https://repository.tudelft.nl/islandora/object/uuid%3A211d5e4e-bf11-4c71-8a43-6c43a5ce45a4.
[32] L.F.M. da Silva, P.J.C. das Neves, R.D. Adams, J.K. Spelt, Analytical models of adhesively bonded joints—Part I: literature survey, Int. J. Adhesion Adhes. 29 (2009) 319–330, https://doi.org/10.1016/j.ijadhadh.2008.06.005.
[33] L.F.M. da Silva, A. Öschner, R.D. Adams (Eds.), Handbook of Adhesion Technology (2 Volumes, second ed., Springer, Heidelberg (DE), 2018.
[34] L.D.C. Ramalho, R.D.S.G. Campilho, J. Belinha, L.F.M. da Silva, Static strength prediction of adhesive joints: a review, Int. J. Adhesion Adhes. 96 (2020), 102451, https://doi.org/10.1016/j.ijadhadh.2019.102451.
[35] K. Tserpes, A. Barroso-Caro, P.A. Carraro, V.C. Beber, I. Floros, W. Gamon, M. Kozłowski, F. Santandrea, M. Shahverdi, D. Skejić, C. Bedon, V. Rajčić, A review on failure theories and simulation models for adhesive joints, J. Adhes. (2021), https://doi.org/10.1080/00218464.2021.1941903 in press.
[36] I.U. Ojalvo, H.L. Eidinoff, Bond thickness effects upon stresses in single-lap adhesive joints, AIAA J. 16 (3) (1978) 204–211, https://doi.org/10.2514/3.60878.
[37] D.W. Oplinger, A Layered Beam Theory for Single Lap Joints, US Army Materials Technology Laboratory, Technical Report MTL TR 91-23 (1991) Watertown (MS).
[38] D.W. Oplinger, Effects of adherend deflections in single lap joints, Int. J. Solid Struct. 31 (18) (1994) 2565–2587, https://doi.org/10.1016/0020-7683(94)90037-X.
[39] M.Y. Tsai, J. Morton, An evaluation of analytical and numerical solutions to the single lap joints, Int. J. Solid Struct. 31 (1994) 2537–2563, https://doi.org/10.1016/0020-7683(94)90036-1.
[40] Q. Luo, L. Tong, Fully-coupled nonlinear analysis of single lap adhesive joints, Int. J. Solid Struct. 44 (2007) 2349–2370, https://doi.org/10.1016/j.ijsolstr.2006.07.009.
[41] Q. Luo, L. Tong, Analytical solutions for adhesive composite joints considering large deflection and transverse shear deformation in adherends, Int. J. Solid Struct. 45 (2008) 5914–5935, https://doi.org/10.1016/j.ijsolstr.2008.07.001.
[42] Q. Luo, L. Tong, Analytical solutions for nonlinear analysis of composite single-lap adhesive joints, Int. J. Adhesion Adhes. 29 (2009) 144–154, https://doi.org/10.1016/j.ijadhadh.2008.01.007.
[43] J. Wang, C. Zhang, Three-parameter, elastic foundation for analysis of adhesively bonded joints, Int. J. Adhesion Adhes. 29 (2009) 495–502, https://doi.org/10.1016/j.ijadhadh.2008.10.002.
[44] S. Cheng, D. Chen, Y. Shi, Analysis of adhesive-bonded joints with nonidentical adherends, J. Eng. Mech. 117 (3) (1991) 605–623, https://doi.org/10.1061/(ASCE)0733-9399(1991)117:3(605).
[45] J.H. Williams, Stresses in adhesive between dissimilar adherends, J. Adhes. 7 (2) (1975) 97–107, https://doi.org/10.1080/00218467508075042.
[46] W.J. Renton, J.R. Vinson, Analysis of adhesively bonded joints between panels of composite materials, J. Appl. Mech. 44 (1977) 101–106, https://doi.org/10.1115/1.3423971.
[47] F. Delale, F. Edogan, M.N. Aydinoglu, Stresses in adhesively bonded joints: a closed-form solution, J. Compos. Mater. 15 (3) (1981) 249–271, https://doi.org/10.1177/002199838101500305.

[48] D.A. Bigwood, A.D. Crocombe, Elastic analysis and engineering design formulae for bonded joint, Int. J. Adhesion Adhes. 9 (4) (1989) 229–242, https://doi.org/10.1016/0143-7496(89)90066-3.
[49] D.A. Bigwood, A.D. Crocombe, Non-linear analysis adhesive bonded joint design analysis, Int. J. Adhesion Adhes. 10 (1) (1990) 31–41, https://doi.org/10.1016/0143-7496(90)90025-S.
[50] J.L. Högberg, Mechanical Behaviour of Single-Layer Adhesive Joints, Chalmers University of Technology, Thesis for the degree of licentiate of engineering, 2004. Göteborg (SW), http://his.diva-portal.org/smash/record.jsf?pid=diva2%3A32315&dswid=-5623.
[51] K.S. Alfredsson, J.L. Högberg, A closed-form solution to statically indeterminate adhesive joint problems—exemplified on ELS-specimens, Int. J. Adhesion Adhes. 28 (2008) 350–361, https://doi.org/10.1016/j.ijadhadh.2007.10.002.
[52] P. Weißgraeber, N. Stein, W. Becker, A general sandwich-type model for adhesive joints with composite adherends, Int. J. Adhesion Adhes. 55 (2014) 56–63, https://doi.org/10.1016/j.ijadhadh.2014.06.009.
[53] X. Liu, Y. Huang, Z. Yin, S. Bennati, P.S. Valvo, A general solution for the two-dimensional stress analysis of balanced and unbalanced adhesively bonded joints, Int. J. Adhesion Adhes. 54 (2014) 112–123, https://doi.org/10.1016/j.ijadhadh.2014.05.011.
[54] D.J. Allman, A theory for elastic stresses in adhesive bonded lap joints, Q. J. Mech. Appl. Math. 30 (4) (1976) 415–436, https://doi.org/10.1093/qjmam/30.4.415.
[55] D. Chen, S. Cheng, An analysis of adhesive-bonded single-lap joints, J. Appl. Mech. 50 (1982) 109–115, https://doi.org/10.1115/1.3166976.
[56] R.D. Adams, V. Mallick, A method for the stress analysis of lap joints, J. Adhes. 38 (1992) 199–217, https://doi.org/10.1080/00218469208030455.
[57] O. Nemes, F. Lachaud, Double-lap adhesive bonded-joints assembles modeling, Int. J. Adhesion Adhes. 30 (2010) 288–297, https://doi.org/10.1016/j.ijadhadh.2010.02.006.
[58] F. Chen, P. Qiao, On the intralaminar and interlaminar stress analysis of adhesive joints in plated beams, Int. J. Adhesion Adhes. 36 (2012) 44–55, https://doi.org/10.1016/j.ijadhadh.2012.03.005.
[59] W. Jiang, P. Qiao, An improved four-parameter model with consideration of Poisson's effect on stress analysis of adhesive joints, Eng. Struct. 88 (2015) 203–215, https://doi.org/10.1016/j.engstruct.2015.01.027.
[60] Y. Du, Y. Liu, F. Zhou, An improved four-parameter model on stress analysis of adhesive layer in plated beam, Int. J. Adhesion Adhes. 91 (2019) 1–11, https://doi.org/10.1016/j.ijadhadh.2019.02.005.
[61] T.H. Nguyen, P. Le Grognec, Analytical and numerical simplified modeling of a single-lap joint, Int. J. Adhesion Adhes. 108 (2021), 102827, https://doi.org/10.1016/j.ijadhadh.2021.102827.
[62] J. Yang, J.F. Chen, J.G. Teng, Interfacial stress analysis of plated beams under symmetric mechanical and thermal loading, Construct. Build. Mater. 23 (2009) 2973–2987, https://doi.org/10.1016/j.conbuildmat.2009.05.004.
[63] T. Sawa, T. Liu, K. Nakano, J. Tanaka, A two-dimensional stress analysis of single-lap adhesive joints of dissimilar adherends subjected to tensile loads, J. Adhes. Sci. Technol. 14 (1) (2000) 43–66, https://doi.org/10.1163/156856100742104.
[64] T.H. Nguyen, P. Le Grognec, Analytical and numerical simplified modeling of a single-lap joint, Int. J. Adhesion Adhes. 108 (2021), 102827, https://doi.org/10.1016/j.ijadhadh.2021.102827.
[65] J.J. Radice, On the decoupled biharmonic airy stress function for the square-end adhesive layer and sandwich structure core, J. Sandw. Struct. Mater. 23 (1) (2018) 23–46, https://doi.org/10.1177/1099636218818624.
[66] Y. Frostig, O.T. Thomsen, F. Mortensen, Analysis of adhesive bonded joints, square-end, and spew fillet-high order theory approach, J. Eng. Mech. 125 (1999) 1298–1307, https://doi.org/10.1061/(ASCE)0733-9399(1999)125:11(1298).
[67] T.P. Lang, P.K. Mallick, Effect of spew geometry on stresses in single lap adhesive joints, Int. J. Adhesion Adhes. 18 (1998) 167–177, https://doi.org/10.1016/S0143-7496(97)00056-0.
[68] J.A. Harris, R.D. Adams, Strength prediction of bonded single lap joints by non linear finite element methods, Int. J. Adhesion Adhes. 4 (2) (1984) 65–78, https://doi.org/10.1016/0143-7496(84)90103-9.
[69] F. Mortensen, O.T. Thomsen, Simplified linear and non-linear analysis of stepped and scarfed adhesive-bonded lap-joints between composite laminates, Compos. Struct. 38 (1–4) (1997) 281–294, https://doi.org/10.1016/S0263-8223(97)00063-9.
[70] F. Mortensen, Development of Tools for Engineering Analysis and Design of High-Performance FRP-Composite Structural Elements, PhD Dissertation, 1998. Aalborg University (SW), https://vbn.aau.dk/ws/portalfiles/portal/316443113/mortensen-flemming.pdf.
[71] F. Mortensen, O.T. Thomsen, Analysis of adhesive bonded joints: a unified approach, Compos. Sci. Technol. 62 (2002) 1011–1031, https://doi.org/10.1016/S0266-3538(02)00030-1.
[72] F. Mortensen, O.T. Thomsen, Coupling effects in adhesive bonded joints, Compos. Struct. 56 (2002) 165–174, https://doi.org/10.1016/S0263-8223(02)00002-8.
[73] A. Kalnins, Analysis of shell of revolutions subjected to symmetrical and non-symmetrical loads, J. Appl. Mech. (1964) 1355–1365, https://doi.org/10.1121/1.1919208.
[74] E. Paroissien, Contribution Aux Assemblages Hybrides (Boulonnés/Collés) – Application Aux Jonctions Aéronautiques, PhD Dissertation, 2006. Université de Toulouse III (FR), http://thesesups.ups-tlse.fr/3/.
[75] E. Paroissien, M. Sartor, J. Huet, F. Lachaud, Hybrid (bolted/bonded) joints applied to aeronautic parts: analytical two-dimensional model of a hybrid (bolted/bonded) single-lap joint, AIAA-2006-2268 47th AIAA/ASME/ASCE/AHS/ASC Structures, Structural Dynamics, and Material Conference, 1-4 May 2006, Newport (RI). https://doi.org/10.2514/6.2006-2268.
[76] E. Paroissien, M. Sartor, J. Huet, Hybrid (bolted/bonded) joints applied to aeronautic parts: analytical one-dimensional models of a single-lap joint, Proceeding on CD-ROM ISBN 2-9523979-1-0 paper No. 34, 6th International Conference on Integrated Design and Manufacturing in Mechanical Engineering AFM 17-19 May 2006 Grenoble (FR).
[77] E. Paroissien, M. Sartor, J. Huet, F. Lachaud, Analytical two-dimensional model of a hybrid (bolted/bonded) single-lap joint, J. Aircraft 44 (2) (2007) 573–582, https://doi.org/10.2514/1.24452.
[78] E. Paroissien, E.M. Sartor, J. Huet, Hybrid (bolted/bonded) joints applied to aeronautic parts: analytical one-dimensional models of a single-lap joint, in: S. Tichkiewitch, M. Tollenaere, P. Ray, Springer (Eds.), The Book: Trends and Recent Advances in Integrated Design and Manufacturing in Mechanical Engineering II, 2007, ISBN 978-1-4020-6760-0, pp. 95–110, https://doi.org/10.1007/978-1-4020-6761-7_7.
[79] E. Paroissien, F. Lachaud, S. Schwartz, A. Da Veiga, P. Barrière, Simplified stress analysis of hybrid (bolted/bonded) joints, Int. J. Adhesion Adhes. 77 (2017) 183–197, https://doi.org/10.1016/j.ijadhadh.2017.05.003.
[80] E. Paroissien, F. Lachaud, On the potential static strength of hybrid (bolted/bonded) lap joints with functionally graded adhesives, AIAA J. 57 (9) (2019) 4093–4103, https://doi.org/10.2514/1.J058372.
[81] E. Paroissien, A. Da Veiga, A. Laborde, An 1D-Beam Approach for Stress Analysis and Fatigue Life Prediction of Bonded Joints, 26th International Committee on Aeronautical Fatigue, 1–3 June 2011, Montréal, CN, Book of Proceedings, Springer Eds., ISBN 978-94-007-1663-6, pp. 359-374. https://doi.org/10.1007/978-94-007-1664-3_29.
[82] E. Paroissien, F. Gaubert, A. Da Veiga, F. Lachaud, Elasto-plastic analysis of bonded joints with macro-elements, J. Adhes. Sci. Technol. 27 (13) (2013) 1464–1498, https://doi.org/10.1080/01694243.2012.745053.
[83] E. Paroissien, F. Lachaud, T. Jacobs, A simplified stress analysis of bonded joints using macro-elements, in: K.L. Mittal, S. Kumar, Wiley (Eds.), The Book: Advances in Modeling and Design of Adhesively Bonded Multilayered Systems, 2013, pp. 93–146, https://doi.org/10.1002/9781118753682.ch4 (Chapter 4).
[84] G. Lélias, E. Paroissien, F. Lachaud, J. Morlier, S. Schwartz, C. Gavoille, An extended semi-analytical formulation for fast and reliable stress analysis of adhesively bonded joints, Int. J. Solid Struct. 62 (2015) 18–39, https://doi.org/10.1016/j.ijsolstr.2014.12.027.
[85] G. Lélias, Adhesively Bonded Joints: Modeling, Simulation and Experimental Characterization, PhD Dissertation, 2016. Université de Toulouse III (FR), https://depozit.isae.fr/theses/2016/2016_Lelias_Guillaume.pdf.
[86] E. Paroissien, L.F.M. da Silva, F. Lachaud, Simplified stress analysis of functionally graded single-lap joints subjected to combined thermal and mechanical loads, Compos. Struct. 203 (2018) 85–100, https://doi.org/10.1016/j.compstruct.2018.07.015.
[87] E. Paroissien, F. Lachaud, L.F.M. da Silva, S. Seddiki, A comparison between macro-element and finite element solutions for the stress analysis of functionally graded single-lap joints, Compos. Struct. 215 (2019) 331–350, https://doi.org/10.1016/j.compstruct.2019.02.070.
[88] S. Schwartz, E. Paroissien, F. Lachaud, General formulation of macro-elements for the simulation of multi-layered bonded structures, J. Adhes. 96 (2019) 602–632, https://doi.org/10.1080/00218464.2019.1622420.
[89] K. Sekmen, E. Paroissien, F. Lachaud, Simplified stress analysis of multilayered adhesively bonded structures, Int. J. Adhesion Adhes. 97 (2020), 102497, https://doi.org/10.1016/j.ijadhadh.2019.102497.
[90] B. Ordonneau, E. Paroissien, M. Salaün, J. Malrieu, A. Guigue, S. Schwartz, Methodology for the computation of the macro-element stiffness matrix for the stress analysis of a lap joint with functionally graded adhesive properties, Int. J. Adhesion Adhes. 97 (2020), 102505, https://doi.org/10.1016/j.ijadhadh.2019.102505.
[91] V. Torrelli, E. Paroissien, Simplified stress analysis of multilayered bonded structure under 1D-bar kinematics, Compos. Struct. 112 (2020), 112641, https://doi.org/10.1016/j.compstruct.2020.112641.
[92] F. Lachaud, E. Paroissien, L. Michel, Validation of a simplified analysis for the simulation of delamination of CFRP composite laminated materials under pure mode I, Compos. Struct. 237 (2020), 111897, https://doi.org/10.1016/j.compstruct.2020.111897.
[93] G.M. Santi, D. Francia, F. Cesari, Explicit analytical shape function calculation for macro-element in glue connection, Mech. Adv. Mater. Struct. (2021), https://doi.org/10.1080/15376494.2021.1992049 in press.
[94] W.C. Carpenter, Finite element analysis of bonded connections, Int. J. Numer. Methods Eng. 6 (3) (1973) 450–451, https://doi.org/10.1002/nme.1620060318.
[95] B. Nageswara Rao, Y.V.K. Sadasiva Rao, S. Yadagiri, Analysis of composite bonded joints, J. Fiber Sci. Technol. 17 (1982) 77–90, https://doi.org/10.1016/0015-0568(82)90037-9.
[96] S. Yadagiri, C. Papi Reddy, T. Sanjeeva Reddy, Viscoelastic analysis of adhesively bonded joints, Comput. Struct. 27 (4) (1987) 445–454, https://doi.org/10.1016/0045-7949(87)90275-6.
[97] H.L. Groth, Calculation of stresses in bonded joints using the substructuring technique, Int. J. Adhesion Adhes. 6 (1) (1986) 31–35, https://doi.org/10.1016/0143-7496(86)90069-2.
[98] W.C. Carpenter, R. Barsoum, Two finite elements for modeling the adhesive in bonded configurations, J. Adhes. 30 (1989) 25–46, https://doi.org/10.1080/00218468908048192.

[99] W.C. Carpenter, A comparison of numerous lap joint theories for adhesively bonded joints, J. Adhes. 35 (1) (1991) 55–73, https://doi.org/10.1080/00218469108030435.
[100] S. Amijima, T. Fujii, A microcomputer program for stress analysis of adhesive-bonded joints, Int. J. Adhesion Adhes. 7 (1987) 199–204, https://doi.org/10.1016/0143-7496(87)90023-6.
[101] M.W. Taylor, Special Finite Elements for Modelling Adhesively Bonded Joints in Two- and Three-Dimensions, Master of Science Dissertation, Virginia Polytechnic Institute and State University, Blacksburg (VA), 1986, http://vtechworks.lib.vt.edu/handle/10919/46413.
[102] R.H. Andruet, D.A. Dillard, S.M. Holzer, Two- and three-dimensional geometrical nonlinear finite elements for analysis of adhesive, Int. J. Solid Struct. 21 (1) (2001) 17–34, https://doi.org/10.1016/S0143-7496(00)00024-5.
[103] P. Schmidt, U. Edlund, Analysis of adhesively bonded joints: a finite element method and a material model with damage, Int. J. Numer. Methods Eng. 66 (8) (2006) 1271–1308, https://doi.org/10.1002/nme.1593.
[104] P. Schmidt, U. Edlund, A finite element method for failure analysis of adhesively bonded structures, Int. J. Adhesion Adhes. 30 (2010) 665–681, https://doi.org/10.1016/j.ijadhadh.2010.05.012.
[105] P. Gustafson, A.M. Waas, A macroscopic finite element for a symmetric double lap joint subjected to mechanical and thermal loading, 16th International Conference on Composite Materials, 8-13 July 2007, Kyoto (JP).
[106] P. Gustafson, Analytical and Experimental Methods for Adhesively Bonded Joints Subjected to High Temperatures, PhD Dissertation, 2008. University of Michigan (IL), https://deepblue.lib.umich.edu/handle/2027.42/60791.
[107] P. Gustafson, A. Bizard, A.M. Waas, A bonded joint finite element for a symmetric double lap joint subjected to mechanical and thermal loads, Int. J. Numer. Methods Eng. 79 (1) (2009) 94–126, https://doi.org/10.1002/nme.2561.
[108] S.E. Stapleton, A.M. Waas, Macroscopic finite element for a single lap joint, AIAA 2009-244950th AIAA/ASME/ASCE/AHS/ASC structures, structural dynamics, and materials conferenc, 4-7 May 2009, Palm Springs (CA), https://hdl.handle.net/2027.42/76219.
[109] S.E. Stapleton, A.M. Waas, B.A. Bednarcyk, Modeling progressive failure of bonded joints using a single joint finite element, AIAA 2010-3100, 51st AIAA/ASME/ASCE/AHS/ASC Structures, Structural Dynamics, and Materials Conference 12-15 April 2010, Orlando (FL). https://ntrs.nasa.gov/api/citations/20110000526/downloads/20110000526.pdf.
[110] S.E. Stapleton, The Analysis of Adhesively Bonded Advanced Composite Joints Using Joint Finite Elements, PhD Dissertation, 2012. University of Michigan (IL), https://deepblue.lib.umich.edu/handle/2027.42/91417.
[111] S.E. Stapleton, A.M. Waas, S.M. Arnold, B.A. Bednarcyk, Corotational formulation for bonded joint finite elements, AIAA J. 52 (2014) 1280–1293, https://doi.org/10.2514/1.J052422.
[112] L.J. Hart-Smith, Adhesive-bonded Scarf and Stepped-Lap Joints, NASA Contractor Report, CR-112235, 1973. Douglas Aircraft Company, Long Beach (CA), https://ntrs.nasa.gov/api/citations/19740005084/downloads/19740005084.pdf.
[113] E. Oterkus, A. Barut, E. Madenci, S.S. Smeltzer, D.R. Ambur, Nonlinear Analysis of Bonded Composite Joints, AIAA-2004-1560, 45th AIAA/ASME/ASCE/AHS/ASC Structures, Structural Dynamics, and Materials Conference, 19-22 April 2004, Palm Springs (CA). https://doi.org/10.2514/6.2004-1560.
[114] R.J.C. Carbas, L.F.M. da Silva, M.L. Madureira, G.W. Critchlow, Modelling of functionally graded adhesive joints, J. Adhes. 90 (8) (2014) 698–716, https://doi.org/10.1080/00218464.2013.834255.
[115] N. Stein, P. Weißgraeber, W. Becker, Stress solution for functionally graded adhesive joints, Int. J. Solid Struct. 97–98 (2016) 300–311, https://doi.org/10.1016/j.ijsolstr.2016.07.019.
[116] N. Stein, J. Felger, W. Becker, Analytical models for functionally graded adhesive joints: a comparative study, Int. J. Adhesion Adhes. 76 (2017) 70–82, https://doi.org/10.1016/j.ijadhadh.2017.02.001.
[117] B. Ordonneau, Méthodologies pour la simulation rapide et fiable de structures collées multi-couches sous sollicitation dynamique, PhD Dissertation, 2021. Université de Toulouse III (FR).
[118] T. Swift, in: J.B. Chang, J.L. Rudd (Eds.), Fracture Analysis of Stiffened Structure. Damage Tolerance of Metallic Structures: Analysis Methods and Application, ASTM STP 842, 1984, pp. 69–107.
[119] H. Huth, Influence of Fastener flexibility on the prediction of load transfer and fatigue life for multiple row joints, in: John M. Potter (Ed.), Fatigue in Mechanically Fastened Composite and Metallic Joints, ASTM STP 927, 1986, pp. 221–250. Philadelphia (PA.
[120] D.A. Cope, T.E. Lacy, Stress intensity determination in lap joints with mechanical fasteners. AIAA-2000-1368, 41st AIAA/ASME/ASCE/AHS/ASC Structures, Structural Dynamics, and Materials Conference, , 3-6 April 2000, Atlanta (GA). https://doi.org/10.2514/6.2000-1368.
[121] A. A. Hartman, Fatigue Tests on Single-Lap Joints in Clad 2024-T3 Aluminium Alloy Manufactured by a Combination of Riveting and Adhesive Bonding, NLR TN M2170, Amsterdam (NL), 1966.
[122] M. Imanaka, K. Haraga, T. Nishikawa, Fatigue strength of adhesive/rivet combined lap joints, J. Adhes. 49 (1995) 197–209, https://doi.org/10.1080/00218469508014356.
[123] M. Fu, P.K. Mallick, Fatigue of hybrid (adhesive/bolted) joints in SRIM composites, Int. J. Adhesion Adhes. 21 (2001) 145–159, https://doi.org/10.1016/S0143-7496(00)00047-6.
[124] G. Kelly, Joining of Carbon Fibre Reinforced Plastics for Automotive Applications, PhD Dissertation, Royal Institute of Technology (SW), 2004, http://www.diva-portal.org/smash/get/diva2:9674/FULLTEXT01.pdf.
[125] G. Kelly, Quasi-static strength and fatigue life of hybrid (bonded/bolted) composite single-lap joints, Compos. Struct. 72 (2006) 119–129, https://doi.org/10.1016/j.compstruct.2004.11.002.
[126] J.K. Kweon, J.W. Jung, T.H. Kim, J.H. Choi, D.H. Kim, Failure of carbon composite-to-aluminium joints with combined fastening and adhesive bonding, Compos. Struct. 75 (2006) 192–198, https://doi.org/10.1016/j.compstruct.2006.04.013.
[127] S. Gómez, J. Oñoro, J. Pecharromán, A simple mechanical model of a structural hybrid adhesive/rivet single lap joint, Int. J. Adhesion Adhes. 27 (4) (2007) 236–267, https://doi.org/10.1016/j.ijadhadh.2006.01.004.
[128] R. Matzuzaki, M. Shibata, A. Todoroki, Improving performance of GFRP/aluminum single lap joints using bolted/co-cured hybrid method, Compos. Part A Appl. Sci. Manuf. 39 (2008) 154–163, https://doi.org/10.1016/j.compositesa.2007.11.009.
[129] B. Kumar, C.T. Sun, P.H. Wang, R. Sterkenburg, Adding additional load paths in a bonded/bolted hybrid joint, J. Aircraft 47 (5) (2010) 1593–1598, https://doi.org/10.1016/j.ijadhadh.2010.01.005.
[130] C.T. Hoang-Ngoc, E. Paroissien, Simulation of single-lap bonded and hybrid (bolted/bonded) joints with flexible adhesive, Int. J. Adhesion Adhes. 30 (2010) 117–129, https://doi.org/10.1016/j.ijadhadh.2009.12.002.
[131] T. Sadowski, M. Knéc, P. Golewski, Experimental investigations and numerical modeling of steel adhesive joints reinforced by rivets, Int. J. Adhesion Adhes. 30 (2010) 338–346, https://doi.org/10.1016/j.ijadhadh.2009.11.004.
[132] F. Moroni, A. Pirondi, F. Kleiner, Experimental analysis and comparison of the strength of simple and hybrid structural joints, Int. J. Adhesion Adhes. 30 (2010) 367–379, https://doi.org/10.1016/j.ijadhadh.2010.01.005.
[133] J.F. Ramière, C. Briançon, F. Chéret, J.P. Jeandrau, M. Leroy, J. Renard, A. Thionnet, Jonctions hybrides boulonnées-collées. Application aux cas des structures d'avions, Rev. des Compos. et des Mater. Av. 20 (2) (2010) 215–232, https://doi.org/10.3166/rcma.20.215-232.
[134] M. Leroy, Expérimentation et modélisation du comportement mécanique de structures marines collées et aéronautiques collées-boulonnées, PhD Dissertation, 2011. Mines ParisTech (FR), https://pastel.archives-ouvertes.fr/pastel-00732181/document.
[135] M. Samaei, M. Zehsaz, T.N. Chakherlou, Experimental and numerical study of fatigue crack growth of aluminum alloy 2024-T3 single lap simple bolted and hybrid (adhesive/bolted) joints, Eng. Fail. Anal. 59 (2016) 253–268, https://doi.org/10.1016/j.engfailanal.2015.10.013.
[136] K. Bodjona, K. Raju, G.H. Lim, L. Lessard, Load sharing in single-lap bonded/bolted composite joints. Part I: model development and validation, Compos. Struct. 129 (2015) 268–275, https://doi.org/10.1016/j.compstruct.2015.04.040.
[137] K. Bodjona, Mechanics of Hybrid Bonded-Bolted Joints, PhD Dissertation, 2016. McGill University (QC), https://escholarship.mcgill.ca/concern/theses/1v53k0709.
[138] K. Bodjona, L. Lessard, Hybrid bonded-fastened joints and their application in composite structures: a general review, J. Reinforc. Plast. Compos. 35 (9) (2016) 764–781, https://doi.org/10.1177/0731684415627296.
[139] J.I. Choi, S.M. Hasheminia, H.J. Chun, J.C. Park, Experimental study on failure mechanism of hybrid composite joints with different adhesives, Fibers Polym. 18 (18) (2017) 569–574, https://doi.org/10.1007/s12221-017-1148-z.
[140] G.H. Lim, K. Bodjona, K. Raju, V. Romanov, S. Fielding, L. Lessard, Evolution of mechanical properties of flexible epoxy adhesives under cyclic loading and its effects on composite hybrid bolted/bonded joint design, Compos. Struct. 189 (2018) 54–60, https://doi.org/10.1016/j.compstruct.2018.01.049.
[141] G.H. Lim, M. Heidari-Rarani, K. Bodjona, K.P. Raju, V. Romanov, L. Lessard, Mechanical characterization of a flexible epoxy adhesive for the design of hybrid bonded-bolted joints, Polym. Test. 79 (2019), 106048, https://doi.org/10.1016/j.polymertesting.2019.106048.
[142] F. Gamdani, R. Boukhili, A. Vadean, Tensile behavior of hybrid multi-bolted/bonded joints in composite laminates, Int. J. Adhesion Adhes. 95 (2019), 102426, https://doi.org/10.1016/j.ijadhadh.2019.102426.
[143] G. Lélias, E. Paroissien, F. Lachaud, J. Morlier, Experimental characterization of cohesive zone models for thin adhesive layers loaded in mode I, mode II, and mixed-mode I/II by the use of a direct method, Int. J. Solid Struct. 158 (2019) 90–115, https://doi.org/10.1016/j.ijsolstr.2018.09.005.
[144] A. Turon, P.P. Camanho, J. Costa, J. Renart, Accurate simulation of delamination growth under mixed-mode loading using cohesive elements: definition of interlaminar strengths and elastic stiffness, Comps. Struct. 92 (8) (2010) 1857–1864, https://doi.org/10.1016/j.compstruct.2010.01.0125.
[145] E. Oterkus, A. Barut, E. Madenci, D.R. Ambur, Analysis of bolted-bonded composite lap joints, 48th AIAA/ASME/ASCE/AHS/ASC Structures, Structural Dynamics, and Materials Conference, 23-26 April 2007, Honolulu (HI). https://doi.org/10.2514/6.2007-2187.
[146] H. Schonhorn, F.W. Ryan, T.T. Wang, Effects of symmetrical bonding defects on tensile shear strength of lap joints having ductile adhesives, J. Appl. Polym. Sci. 15 (5) (1971) 1069–1078, https://doi.org/10.1002/app.1971.070150503.
[147] H. T.T. Wang, F.W. Ryan, H. Schonhorn, Effects of symmetrical bonding defects on tensile shear strength of lap joints having brittle adhesives J. Appl. Polym. Sci. 16 (8) (1972) 1901–1909, https://doi.org/10.1002/app.1972.070160804.